BABES-BOLYAI UNIVERSITY
FACULTY OF PHYSICS

DOCTORAL SCHOOL OF PHYSICS

MAGNETIC PROPERTIES AND MAGNETOCALORIC EFFECT ON SELECTED RARE EARTH – TRANSITION METAL INTERMETALLIC COMPOUNDS

Thesis Summary

PhD Student,
Simu V. Gabriela (căs. Souca)

Scientific Adviser,
Prof. Dr. Romulus V. Tetean

Cluj-Napoca
-2022-

Thesis Contents

Abstract

Rare earth – transition metal intermetallic compounds form a highly important class of materials, which gained a major interest in the research field due to their practical applications in industry and their remarkable importance in our daily life. In this work we succeeded to point out some physical properties of $Ce_{1-x}Y_xFe_2$, $Gd_{1-x}Ce_xCo_2$, $GdCo_{2-x}A_x$ (*A*=Ni, Cu, Al and Mn) Laves phase type intermetallic compounds, additionally to the existing researches on this class of compounds. The dopant concentration was chosen in order to adjust the magnetic transition temperature as close as possible to room temperature. In order to get a deep understanding of the physical properties of the transition metal, different analysis have been combined: magnetic measurements, X-ray Diffraction (XRD), X-ray photoelectron spectroscopy (XPS) and band structure calculations. A full evaluation of magnetocaloric properties was carried out in order to check the possibility to use the investigated systems in magnetic refrigeration field. The calculated relative cooling power, *RCP(S)*, normalized relative cooling power at the applied magnetic field, $RCP(\Delta S)/\Delta B$, and temperature-averaged entropy change, TEC parameters show that these compounds could be promising candidates for applications in magnetic refrigeration devices.

Keywords: Laves phases, electronic structure, intermediate valence, magnetic properties, magnetocaloric effect, band structure calculations

Introduction

In recent decades, magnetic materials could be labelled as a fundamental item on which modern technology relies on. Magnetic materials are components of a great number of electromechanical and electronic devices. As an example, in recent years, in most cases, the classical electromagnetic core in motors has been replaced by strong permanent magnets. The significant progress made in the fields such as information technology, telecommunications or advancements in household technology is attributed in large amounts to the development of advanced magnetic materials. A large number of magnetic materials are used as components in magnetic refrigerators, replacing conventional vapor-gas cycles with magnetic refrigeration cycles.

The purpose of this thesis is to improve the list of magnetic material which can be use as magnetic refrigerators and moreover to bring additional information about the structural, electronic and magnetic properties of the presented materials, that can be used for the future research. The thesis itself is structured on six chapters.

The first chapter is containing some theoretical considerations regarding rare earth – transition metal intermetallic compounds and a short description of magnetocaloric effect in intermetallic compounds.

The second chapter is presenting the experimental techniques used in order to obtain the magnetic materials, to perform structural characterization and to investigate the electronic structure, magnetic properties and magnetocaloric effect.

The third chapter is providing further information on the magnetic and electronic properties in $Ce_{1-x}Y_xFe_2$ (x = 0.1, 0.15, 0.2, 0.25), as well asa full evaluation of magnetocaloric effect around romm temperature.

Chapter four contains detailed analyses of magnetic properties and magnetocaloric effect for $Gd_{1-x}Ce_xCo_2$ (x = 0.1, 0.15, 0.2, 0.25, 0.3, 0.4, 0.5, 0.6, 0.75, 0.8 and 0.9) intermetallic compounds.

Chapter five present a detailed correlated study of structural, electronic, and magnetic properties of $GdCo_{2-x}A_x$ Laves phase intermetallic compounds (A = Ni, Mn, Cu and Al). In view of potential applications in magnetic refrigeration, a full evaluation of magnetocaloric properties was accomplished for the compounds with substitutional A = Ni, Cu and Al.

Finally, the general ***conclusions*** of the thesis are presented..

Chapter 1

Rare earth – 3d Transition metal intermetallic compounds

Rare earth – transition metal intermetallic compounds form a highly important class of materials, which gained a major interest in the research field due to their practical applications in industry and their remarkable importance in our daily life. The number of these compounds is huge, taking into consideration that one rare earth element and one 3*d* element can form more than ten different intermetallic compounds, with different structural arrangement and physical properties.

The crystallographic structure and chemical composition of *R-M* intermetallic compounds establish some of the intrinsic magnetic properties of them like saturation magnetization, Curie

temperature and magnetocrystalline anisotropy. The microstructure of *R-M* intermetallic compounds determines their extrinsic magnetic properties like coercivity and remanent magnetization. Altogether, the magnetic properties induce the *R-M* intermetallic compounds applications. Several members from this class of compounds have been classified as hard intermetallics, characterized by large hysteresis used as starting materials for permanent magnets of exceptional quality. Semi-hard intermetallics are used for high-density magnetic recording and soft ones having a small hysteresis loop are used in electromagnetic machines [1]. Moreover, it has been discovered that couple compounds have outstanding properties with respect to reversible absorption of hydrogen gas at room temperature and nearly atmospheric pressures. Absorbed densities of about twice the density of liquid hydrogen have been reached.

The magnetic refrigeration technology which is based on magnetocaloric effect of the magnetic compounds has been considered as one of the most encouraging possible methods to our present well used gas compression/expansion technology being an environment friendly alternative with high energy efficiency. Therefore, the magnetocaloric effect of a large class of *R-M* intermetallic compounds have been intensively studied around their Curie temperature [2-4].

Chapter 2

Experimental and characterization techniques

2.1. Sample preparation

Formation of the intermetallic compounds is conditioned by the meltig points and by the direct union of the constituent elements which require a temperature between 200 ºC and 3000 ºC [5]. The different properties of the combining elements and their different range of solid solubility is an often difficulty encountered in preparing certain intermetallic compunds within single phase region. Because of the high reactivity of most metals at raised temperature, the preparation of an intermetallic compound is best regarded as a multicomponent reaction that is likely to involve container materials and atmosphere in contact with the elements.

2.1.1. Arc melting technique

A widly used technique in research laboratories for the preparation of intermetallics which easly can attain temperature up to 3000ºC is arc melting method. The arc melting furnace from Babes Bolyai Univesity, Ioan Ursu Insitute is connected to a DC power source which provides 80V and currents with intensities of up to 100A. The cathode is a tungsten electrode connected to the power source and the anode is the water-cooled cooper furnace heart. The arc is produced by a stream of electrons emitted from the cathode and drawn through plasma of ionized gas to the anode, where high purity starting elements are placed in some small delves. The hearth is isolated from the outside by a heat-resistant glass with rubber seals at both ends. During melting, the whole system is constantly cooled by water circuit and is using argon atmosphere at reduced pressure (20 to 40 cm Hg). To ensure a pure argon atmosphere the chamber is cleaned several times by washing with argon gas. The first step before the melting of constituents begins is to examine the atmosphere by melting a titanium ball located inside the furnace.

2.1.2. Induction melting technique

Another well-known laboratory technique was used in order to prepare intermetallic compounds presented in this work, namely induction melting. The heating of the furnace is produced and controlled by applying a high frequency electromagnetic field. The starting elements are placed in a water-cooled cooper crucible consisting of independent elements, thus the magnetic field lines won't be close and the energy dissipation inside the furnace is reduced. The resultant electric force generated by the coils is opposite to the gravitation therefore the molten is levitating in the middle of the furnace, therefore the rotate of the sample after each melting, for obtaining homogeneous sample, become easier. The entire set up is connected to a gas and vacuum inlet permitting a melting process under high purity argon atmosphere.

2.2. Structural characterization

The structural characterization of the compounds was performed using X-ray powder diffraction method. In our case a Bruker AXS D8 Advance powder diffractometer with Cu Kα radiation was used for the data acquisition at room temperature. The entire set up is connected to a computer, that through the software, enables the user to acquire and analyze data. Rietveld refinement can be employed for the qualitative analysis of the XRD patterns [6].

2.3. X-Ray Photoelectron Spectroscopy

X-Ray Photoelectron Spectroscopy (XPS) is one of the most widely used methods for exploring the electronic structure of atoms, molecules and condensed matter [7, 8]. The energy of the incoming X-ray radiation is $h\nu > 1000$ eV and E_{kin} explored by XPS techniques is for the photoelectrons emitted from inner levels of a solid or from the outermost occupied band.

The XPS investigations were performed at the Osnabrück University using a commercially available spectrometer PHI Model 5600 Multi-Technique System produced by the Perkin Elmer Corporation. In order to avoid surface contamination, the bulk samples were crushed in situ in the preparation chamber in high–vacuum conditions (usually around $7x10^{-8}$torr), before being transferred to the main chamber where the measurements were performed. The Al X-ray anode was used for all measurements with monochromatic radiation. The characteristic energy and half–widths for the Al Kα radiation are: 1486.6 eV and 0.3 eV. The photoemitted electrons were filtered according to their energy using an 11 inches hemispherical condenser. A multi-channel detector with 16 channel plates was used for the detection of the photoelectrons. All components of the main chamber are kept under UHV during the measurements by using a combination of suitable vacuum pumps: turbomolecular, sputter and sublimation pumps. In order to avoid surface contamination over the experiments, a base pressure of about 10^{-10} torr was kept in the main chamber during the recording of the XPS spectra presented in this work.

2.4. Magnetic measurements

The most commonly used type of magnetometer is the Vibrating Sample Magnetometer (VSM). VSM is recording the magnetic moment of the investigated materials as a function of magnetic field (up to 12T) and temperature (1.4 K – 650 K). The running principle is based on Faraday's law which states that an electromagnetic field will be generated in a coil when there is a change in flux linking the coil. The sample to be studied is placed in the constant magnetic field, supplied by the electromagnet, which

will magnetize the sample. Therefore, the magnetization of the sample increases with the strength of the constant magnetic field. The sample is attached to the end of a nonmagnetic rod, the other end of which is fixed to a mechanical vibrator. The sample rod can be rotated in order to get the wanted orientation of the sample to the constant magnetic field. The oscillating magnetic field of the moving sample induces an alternating electromagnetic field in the detection coils, whose magnitude is proportional to the magnetic moment of the sample. The small alternating electromagnetic field is amplified, usually with a lock-in amplifier which is sensitive only to signals at the vibration frequency [9]. The detection-coil arrangement involves balanced pairs of coils that cancel signals due to variation in the applied field. The apparatus is calibrated with a specimen of known magnetic moment, which must be of the same size and shape as the sample to be measured, and should also be of similar permeability [9].

2.5. Band structure calculations

The local density approximation (LDA) was first proposed by Kohn and Sham in 1965 and since then is the highly employed approximation to the exchange-correlation energy. The basic principle behind LDA assume that a general inhomogeneous system is locally homogeneous in order to use the exchange-correlation hole corresponding to the homogeneous electron gas, which is known to an exquisite accuracy [10].

Rare-earth metal compounds are distinguished by well localized *d* and *f* orbitals [10]. This localization goes to strong on-site correlations, such that if an electron is occupying a state localized in a particular site, placing a second electron in the same site is penalized with an additional energy, orbitals [10]. This idea was originally crystallized at the level of an empirical Hamiltonian by Hubbard [11]. The Hubbard phenomenological approach has been combined with density-functional calculations by supplementing the LDA with a Hubbard-type onsite repulsion term (LDA+U) [12]. This model produces a splitting into lower and upper Hubbard sub-bands, where the eigenvalues are given by [10]:

$$\varepsilon_i = \frac{\partial E_{LDA+U}}{\partial f_i} = \varepsilon_{LDA} + U\left(\frac{1}{2} + f_i\right)$$

The energy separation is given by the U parameter. The determination of the Hubbard U parameter can be done empirically, by fitting it to experimental data, or by estimating it from LDA calculations from the total energies obtained by varying the occupancy of localized d or f orbitals [10]. Within the LDA+U approach, the Hubbard term is treated at the mean-field level [10].

The KKR method is a multiple-scattering method introduced by Korringa (1947) and Kohn and Rostoker (1954). The starting point of the method is the partitioning of the system into spheres and interstitial regions [10]. The spherical regions are usually called muffin-tin spheres, their radius being the muffin-tin radius, $S_{\vec{R}}$ [10]. The potential is assumed to be spherically symmetric inside the muffin-tin spheres (close to the core) and flat (constant) in the interstitial regions.

By using the computational methods mentioned above, we can determine total energy values, magnetic moments per atom, densities of states (DOS), equilibrium lattice parameters and various information on the band structure for a given compound.

Chapter 3

Structural, magnetic properties and magnetocaloric effect in $Ce_{1-x}Y_xFe_2$ compounds

The Laves phase alloys RFe_2, RCo_2 and RNi_2 exist for the whole rare-earth series. $CeFe_2$ is a particularly interesting because of its anomalously low ferromagnetic ordering temperature (~230 K) and low saturation magnetization at 4.2 K (~2.3 μ_B/f.u) compared to other isostructural compounds [13-15], due to the strong hybridization of the Ce *4f* states with the Fe *3d* valence states [16,17]. It was shown in previous studies that at low temperatures $CeFe_2$ is located near the instability of ferromagnetism, antiferromagnetic spin correlation occurring at low temperatures [18-21].

Many studies were performed on $CeFe_2$ doped with rare – earth, as Gd, Tb, Er, Ho, showing that the Ce and Fe magnetic moments are coupling antiferromagnetically and the Curie temperature is increasing with dopant concentration [22-25]. Due to the variation of the *4f* -occupation number, to the nature of the *4f* state and the degree of Fe *3d* – Ce *4f* coupling a change of the Ce valence was revealed in most of the $Ce_{1-x}R_xFe_2$ explored systems. Consequently, Ce valence is not depending on the atomic size of the dopant element and it fluctuates with concentration of rare earth element. In the investigated systems where the rare earth element is Tb or Dy, a meta-magnetic phase transition can be distinguished, at moderate Ce concentration, revealing the fragility of Ce 4*f* ferromagnetism [24]. The Ce valence fluctuation from the mixed-valence state to the localized state increases the moments of both the Ce and the Fe ions, and enhances the degree of Fe–Fe coupling, leading to the increase of the Curie temperature [25].

There are some reports on the magnetocaloric properties of $Ce_{1-x}R_xFe_2$ compounds [26-28] showing that with the appropriate dopant concentration the magnetocaloric effect can be settled around room temperature, with large magnetic entropy changes of about 17 $Jkg^{-1}K^{-1}$ at 303 K for $Ce_{0.9}Dy_{0.1}Fe_2$ [27].

Previously reported results of the magnetic measurements on $Ce_{1-x}Y_xFe_2$ revealed a roughly linear dependence of the Curie temperature with concentration from 237 K for $CeFe_2$ to 532 K for YFe_2 [29] and a gradually change of Ce valency, without achieving the pure Ce^{3+} state, while the Fe-moment is assumed to be independent of Y substitution [30]. Present research provides further information on the magnetic properties and magnetic moments in $Ce_{1-x}Y_xFe_2$ with x = 0.1, 0.15, 0.2, 0.25.

3.1. Crystalographic analysis of $Ce_{1-x}Y_xFe_2$ intemetallic compounds

The investigated $Ce_{1-x}Y_xFe_2$ samples with x = 0.1, 0.15, 0.2, 0.25 were prepared in the purified argon atmosphere using arc-melting technique and annealed in vacuum at 800 ºC for 5 days and slowly cooled to room temperature. The phase purity of $Ce_{1-x}Y_xFe_2$ compounds was checked using powder X-ray diffraction measurements at room temperature. The registered patterns together with the calculated profiles, using Rietveld refinements run by FULLPROF program [31] are shown in **Figure 3.1.** XRD patterns emphasize that the prepared $Ce_{1-x}Y_xFe_2$ samples are single phase and possess a cubic Laves type structure (C15) with the $Fd\bar{3}m$ space group, specific to $CeFe_2$ phase, where the Ce/Y atoms occupy 8a sites and Fe atoms ocupy 16d sites. Rietveld method on the recorded XRD patterns was used in order to calculate the lattice parameters. The obtained lattice parameters for $Ce_{1-x}Y_xFe_2$ samples show an almost linear increase with the yttrium content, as plotted in **Figure 3.2.**

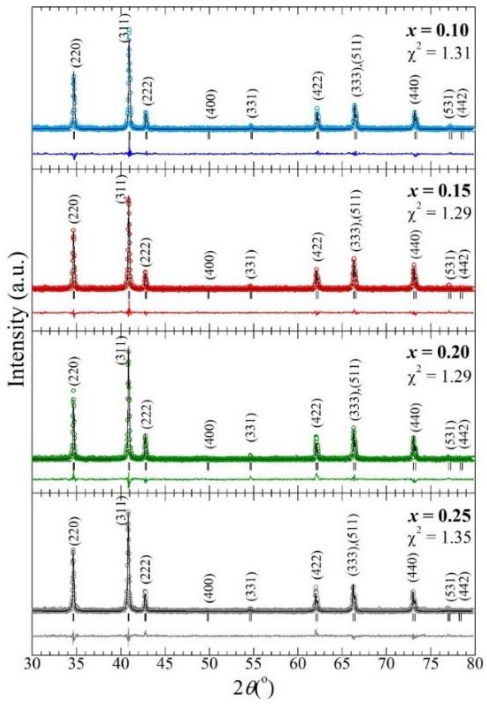

Figure 3.1. XRD patterns of $Ce_{1-x}Y_xFe_2$ samples, together with the calculated profiles using Rietveld method and difference curves [32].

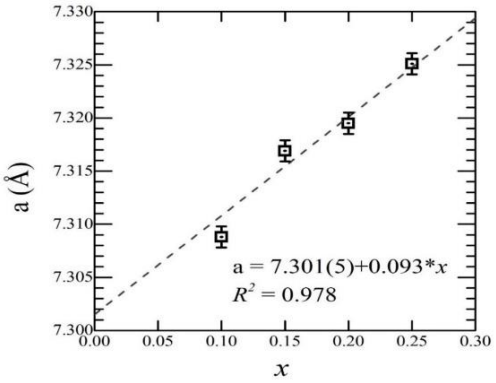

Figure 3.2. The concentration dependence of lattice parameter for $Ce_{1-x}Y_xFe_2$ compounds [32].

3.2. Band structure calculations

The ground state self-consistent electronic structure calculations of $Ce_{1-x}Y_xFe_2$ compounds with $Fd\bar{3}m$ space group and two formula units per unit cell have been carried out by using the tight-binding linear muffin-tin orbital (TB-LMTO) method in the atomic sphere approximation (ASA) [33,34]. All calculations have been performed in the scalar-relativistic limit, i.e. without spin-orbit coupling. Vosko-Wilk-Nusair parameterization has been employed for the exchange-correlation energy [35] within the local spin density approximation (LSDA). The valence basis consists of *s*-, *p*-, *d*- and *f*- type orbitals. The atomic sphere radii used in calculations have been chosen in such a way that overlapping remains within the permissible ASA limit. The tetrahedron method was employed in order to calculate the partial densities of states [36]. The self-consistent calculations were performed for 549 k-points in the irreducible wedge of the Brillouin zone (IBZ) corresponding to 9216 k-points in the full Brillouin zone (BZ). Total energies were calculated within an accuracy of 10^{-2} meV. The ground state was obtained by minimizing the total energy with respect to the unit cell volume.

Based on the experimentally determined lattice parameters the band structures of $Ce_{1-x}Y_xFe_2$ compounds were calculated (**Figure 3.3**). The effect of Y substitution for Ce is the decrease of the state densities near the Fermi level for both spin orientations, as expected considering the gradual increase of lattice parameter and Ce *4f* -Fe *3d* hybridization. The computed iron moments for $Ce_{1-x}Y_xFe_2$ compounds show an increase to about 1.78 μ_B/atom for x = 0.5 and remain above 1.7 μ_B/atom with the increase of Y content, close to the values found in most RFe_2 compounds [37]. The calculated magnetic moments for the Ce and Y atoms on the 8a sites are negative, indicating an antiferromagnetic coupling to the Fe magnetic moments on the 16d sites, and show a very small dependence with the Y concentration (**Figure 3.4**). The values obtained for the magnetic moment at the Y site are around -0.4 μ_B/atom for all concentrations, consistent with the results reported for Y-Fe compounds [38].

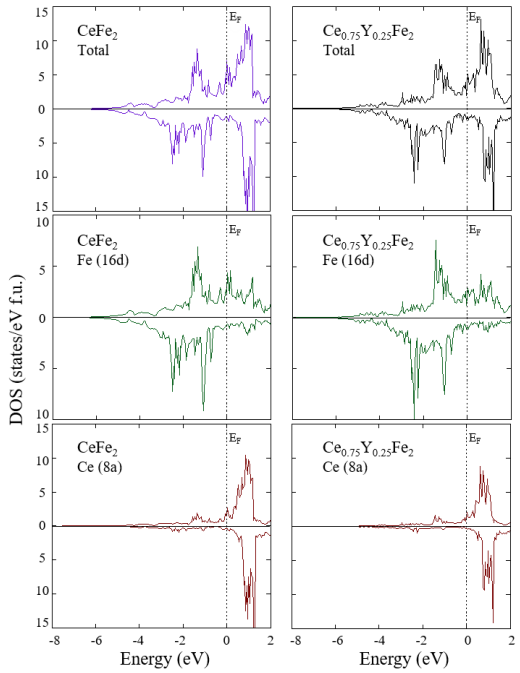

Figure 3.3. Total and partial DOS for $CeFe_2$ and $Ce_{0.75}Y_{0.25}Fe_2$ [32].

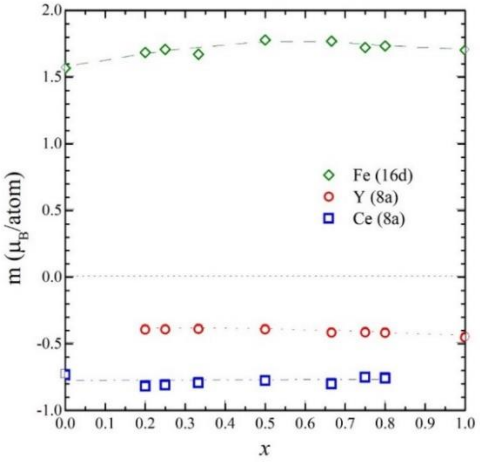

Figure 3.4. The concentration dependence of the calculated magnetic moments for $Ce_{1-x}Y_xFe_2$ [32]

3.3. Magnetic properties and magnetocaloric effect of $Ce_{1-x}Y_xFe_2$ intemetallic compounds

In order to establish the effect of Y substitution, the temperature dependencies of magnetisation in Zero Field Cooled (ZFC) - Field Cooled (FC) modes were register under a small magnetic field of 0.05 T, **Figure 3.5**. The magnetization is increasing with the dopand concentration with an almost linearly trend in the magnetically ordered area and has a sudden transition to the paramagnetic state at Curie temperature. In order to determine the transition temperatures from the magnetic ordered state to the paramagnetic state, the first derivative of magnetization function of temperature was calculated for all samples. The transition temperatures are equal with the minimum value of δM/δT (**Figure 3.6)**.

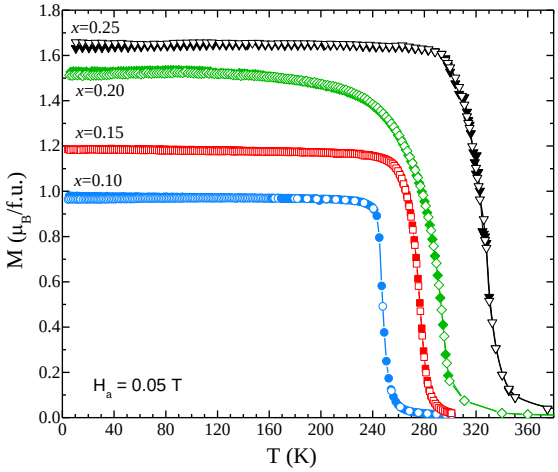

Figure 3.5. Temperature dependence of ZFC (open symbols) and FC (filled symbols) magnetizations in 0.05 T for $Ce_{1-x}Y_xFe_2$

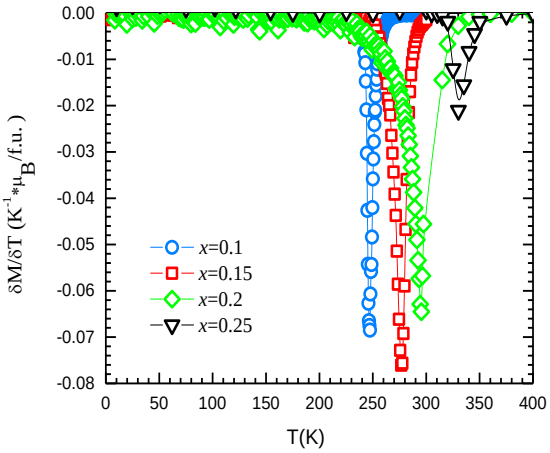

Figure 3.6. The derivative of the magnetizations as a function of temperatures for $Ce_{1-x}Y_xFe_2$ compounds

An almost liniar increase of the obtained Curie temperatures was observed as the concentration of Y is increasing, from 247 K for x = 0.1 to 330 K for x = 0.25. The substitution of Ce by Y modifies the hybridization between Ce *4f* and Fe *3d* states which increases the Fe-Fe direct exchange interaction, permiting the increase of T_c above room temperature.

The samples were subjected to a high magnetic field, up to 12 T, in order to register the magnetization isotherms in a wide temperature range, 4K – 350 K. At T = 4K $Ce_{1-x}Y_xFe_2$ compounds have the same behaviors, saturation being already reached in an applied magnetic field of 1 T, **Figure 3.7**. It can be notice an increasing trend for saturation magnetization with the increasing of ytrium concentration, which is a characteristic of ferrimagnetically ordered materials .

The spontaneous magnetization, *Ms*, for all investigated samples was determined from the measured magnetization isotherms using the approach to saturation law. **Figure 3.8.** shows the temperature dependence of the calculated *Ms* values for all investigated samples.

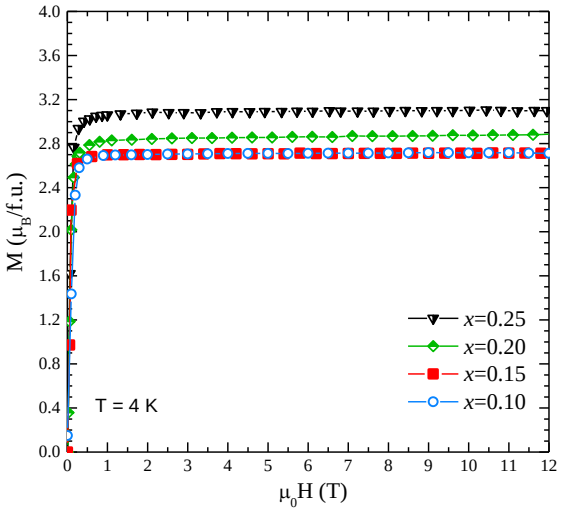

Figure 3.7. Magnetization isotherms for $Ce_{1-x}Y_xFe_2$ compounds recorded at 4 K

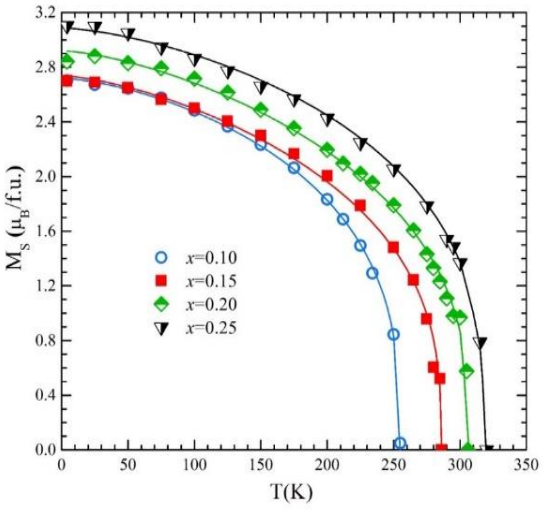

Figure 3.8. The temperature dependence of the saturation magnetization for $Ce_{1-x}Y_xFe_2$ compounds [32].

The calculated value of the spontaneous magnetization at 0 K is increasing with the decrease of Ce content from 2.71 μ_B/f.u for x = 0.1 to 3.08 μ_B/f.u for x = 0.25, indicating an antiferromagnetic coupling between Ce and Fe magnetic moments in the investigated samples. Assuming that for low Y concentration, the magnetic moments for the Ce ions remains roughly the same and has the value of 0.75 μ_B/atom, while the magnetic moment for the Y ions is about 0.4 μ_B/atom, the magnetic moments at the Fe sites were calculated taking into account that the magnetic moments of Fe and Ce/Y are antiparalelly orientated. The obtained values show an increase from 1.71 μ_B/f.u for x = 0.1 to about 1.87 μ_B/Fe atom for x = 0.25, as the hybridization between the Ce *4f* and Fe *3d* states decreases with the Y substitution.

Using the magnetization isotherms measured between 200 K and 380 K with a step of 5 K, the magnetic entropy change was calculated in an external magnetic field of 2 T and 4 T (**Figure 3.9)**. The magnetic entropy change $|\Delta S_m|$ curves display a maximum at a temperature very close to the transition ones. The increase of dopand concentration is causing the decrease of $|\Delta S_m|$ values, while the $|\Delta S_m|$ peaks become broader, a very necessary characteristic for a good refrigerant material. The curves are nearly

symmetric distributed around the transition temperature, characteristic for materials displaying a second order magnetic phase transition [39].

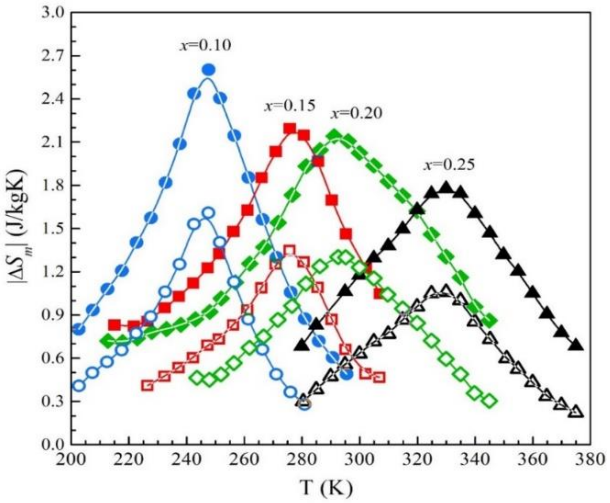

Figure 3.9. The temperature dependence of the magnetic entropy change for $Ce_{1-x}Y_xFe_2$ compounds in an external magnetic field of 2 T (open symbols) and 4 T (filled symbols) [32].

The relative cooling power (RCP) was calculated for all $Ce_{1-x}Y_xFe_2$ compounds in order to evaluate the magnetic refrigeration efficiency. Due to the broad $|\Delta S_m|$ peaks the samples have considerable RCP(S) values, as presented in **Table 3.1**, suggesting that the materials could be used for the magnetic refrigeration applications. Specific normalized cooling power parameter to the variation of magnetic field, $RCP(\Delta S)/\Delta B$, was calculated and the values were listed in **Table 3.1** for all samples. $RCP(\Delta S)/\Delta B$ values for the same composition show no significant change when the applied magnetic field is varied. Therefore, the investigated compounds are suitable for technological applications

***Table 3.1**. Magnetocaloric properties of $Ce_{1-x}Y_xFe_2$ compounds*

x	T_{max} (K)	$\lvert\Delta S_m\rvert$ (J/kgK)		δT_{FWHM} (K)		RCP(S) (J/kg)		RCP(S)/ΔB (J/kgT)	
		0-2 T	0-4 T	0-2 T	0-4 T	0-2 T	0-4 T	0-2 T	0-4 T
0.1	247	1.60	2.55	39	53	62.4	135.1	31.2	33.8
0.15	278	1.33	2.17	50	66	66.5	143.2	33.3	35.8
0.2	294	1.30	2.12	66	82	85.8	173.8	42.9	43.5
0.25	330	1.07	1.78	61	78	65.3	138.8	32.7	34.7

Chapter 4

Electronic structure, magnetic properties and magnetocaloric effect in $Gd_{1-x}Ce_xCo_2$ intermetallic compounds

The present chapter provides additional informations to previous studies [40-42] on pseudobinary $GdCo_2$ compounds and contains detailed analyses of magnetic properties and magnetocaloric effect for $Gd_{1-x}Ce_xCo_2$ intermetallic compounds.

4.1. Crystalographic analysis of $Gd_{1-x}Ce_xCo_2$ intemetallic compounds

The investigated compounds of $Gd_{1-x}Ce_xCo_2$ with x = 0.1, 0.15, 0.2, 0.25, 0.3, 0.4, 0.5, 0.6, 0.75, 0.8 and 0.9 were obtained using arc-melting technique. To compensate the rare earth losses during melting a small excess was added 2 % for Gd and 1% for Ce. The obtained samples were subjected to a heat treatment in quartz tube in vacuum, at 850 ºC for 7 days and slowly cooled to room temperature.

The structure purity of the compounds was checked by X-ray diffraction measurements on grinded samples, at room temperature (**Figure 4.1**). All samples are single phase, with the cubic MgCu2 - Laves type structure, like for GdCo2 and $CeCo_2$.

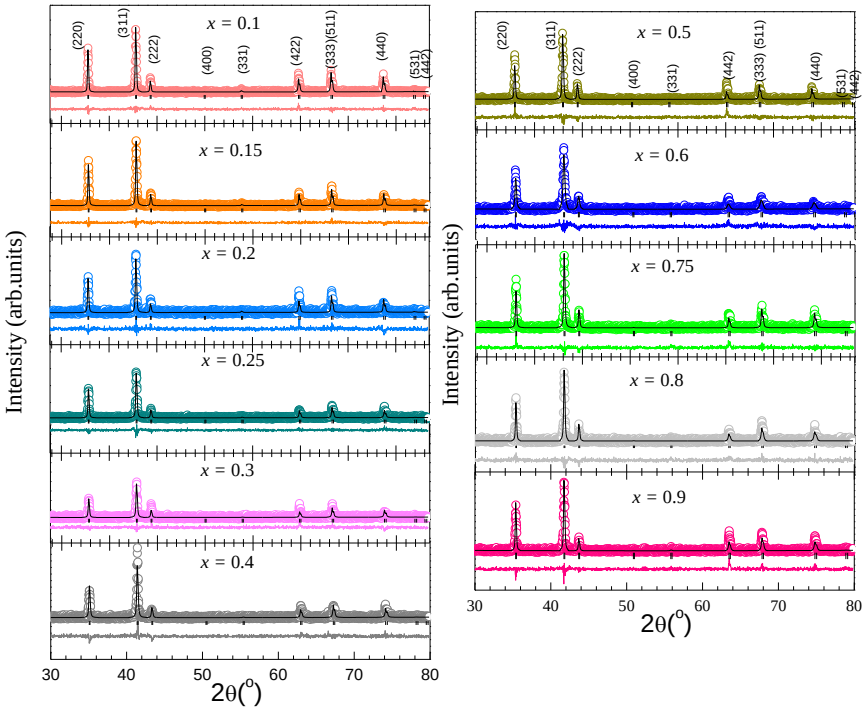

Figure 4.1. XRD patterns of the $Gd_{1-x}Ce_xCo_2$ samples (empty symbols) together with the calculated profile using Rietveld method and difference curves (solid lines)

The refined lattice constant decreases as the Ce content increases, as expected, considering the lattice parameters of GdCo2 (7.247 Å) and CeCo2 (7.162 Å) [43, 44]. The distances between the Co atoms in all investigated compounds are between 2.53 Å and 2.56 Å (**Figure 4.2**), close to those in pure Co metal, namely 2.50-2.51 Å [45]. The unit cell volume calculated using the lattice parameters obtained from Rietveld analysis show an almost linear decrease with the Ce content, as plotted in **Figure 4.2**.

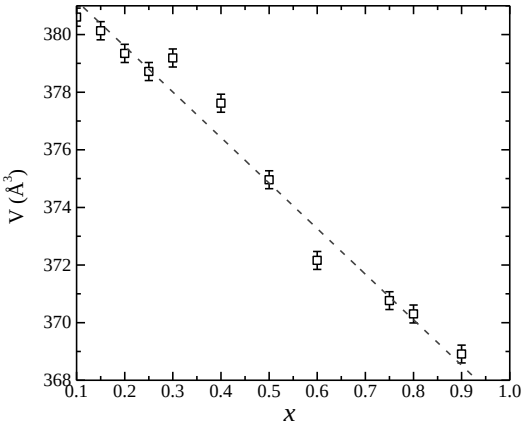

Figure 4.2. The unit cell volume dependence with Ce concentration for $Gd_{1-x}Ce_xCo_2$ samples.

4.2. Electronic structure of $Gd_{1-x}Ce_xCo_2$ intemetallic compounds

Photoemission from Ce 3*d* and 4*d* states give information on the valence state of the Ce atoms. In **Figure 4.3** is represented Ce 3*d* core-level spectra of the investigated $Gd_{1-x}Ce_xCo_2$ compounds with x = 0.4, 0.6, 0.75 and 0.9 which consist of two multiplets corresponding to the spin-orbit split $3d_{5/2}$ and $3d_{3/2}$ core holes. The spin–orbit splitting is about 18.4 eV, for all investigated samples.

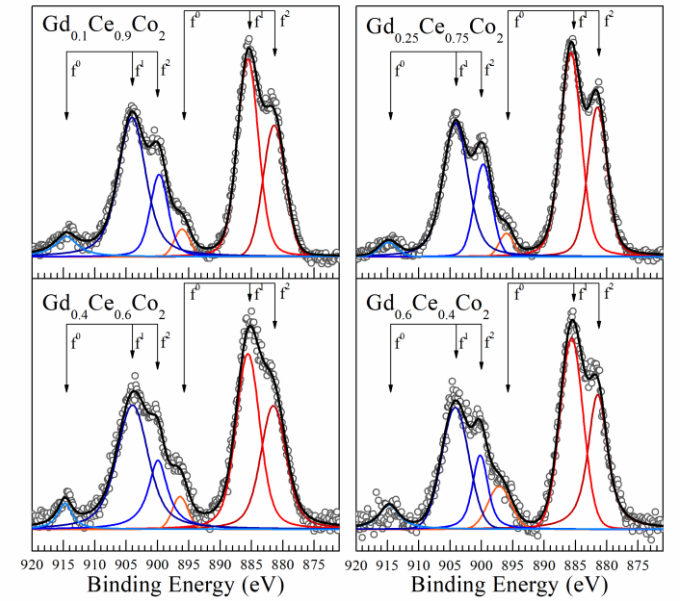

Figure 4.3. Ce 3d core level XPS spectra in $Gd_{1-x}Ce_xCo_2$ (open circles correspond to the experimental spectrum and the continuous curves to the fitting results, after background subtraction) [46].

The multiplet effects due to the coupling of the 3*d* hole with the open 4*f* shell are visible in both the $3d_{5/2}$ and $3d_{3/2}$ peaks, each spin-orbit component being the superposition of spin-orbit-split peaks corresponding to the two initial configurations Ce^{3+} and Ce^{4+}. The line shape analysis shows that the Ce 3*d* XPS consist of six peaks corresponding to the pairs of spin-orbit doublets assigned based on the f^0, f^1, and f^2 configurations [47- 49]. Around 914.7±0.1 eV is the highest binding energy peak which is the result of the $3d^94f^0$ final state, giving proof of the intermediate valence behavior of Ce in the $Gd_{1-x}Ce_xCo_2$ system. The most intense components originating from Ce^{3+} are labelled as f^1, while the lowest energy components marked as f^2 appear due to the strong Coulomb interaction between the 3*d* hole and the electrons located near the Fermi level. These $3d^94f^2$ final-state components originate from the screening of the core hole by the 4*f* electrons, possible due to the hybridization of the Ce 4*f* shell with the conduction band states. The weights of the f^0, f^1, and f^2 configurations are about 7±1 %, 59±1 %, and 34±1% in all $Gd_{1-x}Ce_xCo_2$ investigated samples, close to the values reported for $CeCo_2$ and $CeCo_5$ [49, 50].

The XPS spectra of the Ce 4*d* core levels in $Gd_{1-x}Ce_xCo_2$ compounds, shown in **Figure 4.4**, reflect the mixed valence state of Ce. The Ce 4*d* spectra point out multiplets appearing from the interaction of the 4*d* hole with the 4*f* electrons in the region between 105 and 116 eV binding energy. In the lower binding energy region, between 100 and 110 eV, the peaks corresponding to trivalent Ce are superimposed on the Co 3*s* peaks, while the peaks at higher binding energies, situated at about 119 eV and 122.5 eV, correspond to the fraction of tetravalent Ce in the compound. The spin-orbit splittings for Ce^{4+} are around 3.4±0.1 eV in all investigated samples, in good agreement with the values measured in other mixed valence compounds, such as $CeNi_2$, $CeNi_5$, CeF_4, $Ce_2Co_{15}Mn_3$, $CeCo_7Mn_5$ and $CeCo_8Mn_4$ [50 - 53].

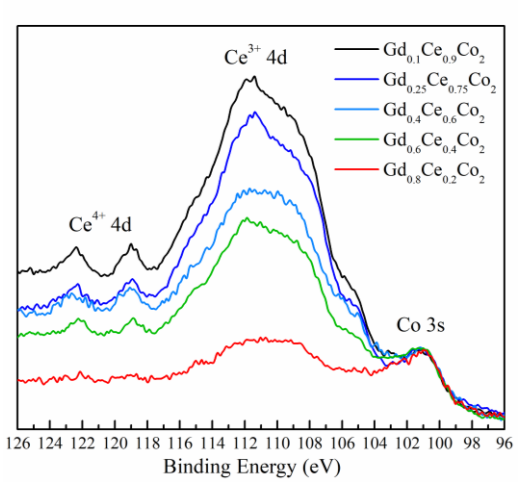

Figure 4.4. XPS spectra of the Ce 4d and Co 3s core levels in $Gd_{1-x}Ce_xCo_2$ [46].

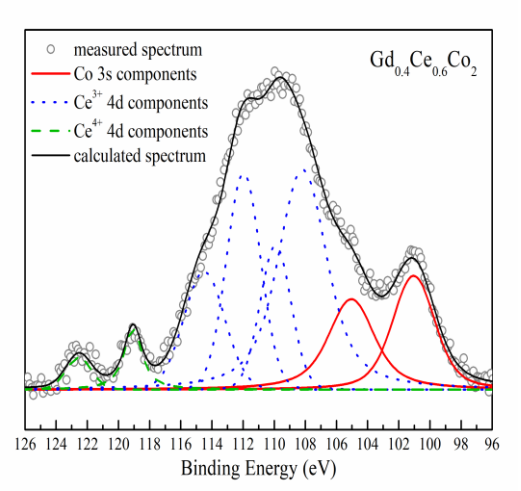

Figure 4.5. XPS spectrum of the Ce 4d and Co 3s core levels in $Gd_{0.4}Ce_{0.6}Co_2$ after background subtraction [46].

The exchange interaction J_{dc} between the core hole spin s and the 3*d* electron spin S gives rise to a satellite on the high binding energy side of the main line of the Co 3*s* spectrum [8]. The exchange splitting is proportional with the Co local moment, hence the splitting between the peaks corresponding to the high spin final state and the low spin final state provides valuable information on the spin moment [54, 55]. The XPS spectra for $Gd_{1-x}Ce_xCo_2$ compounds in the 95 eV to 130 eV binding energy region were fitted after background subtraction with several components, the first two corresponding to the Co 3*s* peaks and the peaks at higher binding energy accounting for the Ce 4*d* multiplet peaks, as presented in **Figure 4.5** for $Gd_{0.4}Ce_{0.6}Co_2$. For all investigated samples an exchange splitting of about 4 eV was found between the high spin final state and the low spin final state of the Co 3*s* core level, which is direct evidence of the local magnetic moments on Co sites. This value is slightly lower than 4.5 eV, found in the pure Co metal [55].

The Co 2*p* XPS spectra for the investigated $Gd_{1-x}Ce_xCo_2$ compounds are shown in **Figure 4.6**. The binding energy of the Co $2p_{1/2}$ and $2p_{3/2}$ core levels in all investigated samples is around 778.2 eV and 793.2 eV, respectively. No significant shift is observed, indicating that the charge transfer can be neglected in this system.

The XPS valence band spectra of $Gd_{1-x}Ce_xCo_2$ compounds shown in **Figure 4.7** are mainly the result of the Co3*d*, Ce5*d* and Ce4*f* states superposition below 4 eV. For all samples the valence band is dominated by the Co 3*d* states, centered at about 1.5 eV, a value close to that observed in pure Co metal (see the inset in Figure 4.8). The contribution from the Ce atoms, although small, can be observed for the samples with higher Ce content. Close to the Fermi level the intensity of the valence band XPS spectra increases with the Ce content due to the Ce $4f^1$ final state contribution, while the feature located at about 2 eV is assigned to the $4f^0$ final state configuration [56]. For Ce mixed valence compounds have shown that the 4*f* state are not far below the Fermi level and both the Ce 5*d* and 4*f* states hybridize with the Co 3*d* states [50,51,56]. It therefore expected that the valence band of $Gd_{1-x}Ce_xCo_2$ compounds is influenced by the same 3*d*-5*d* and 3*d*-4*f* hybridizations. The spectral feature situated at around 8 eV is the contribution of the Gd 4*f* core level and decreases in intensity with increasing Ce concentration.

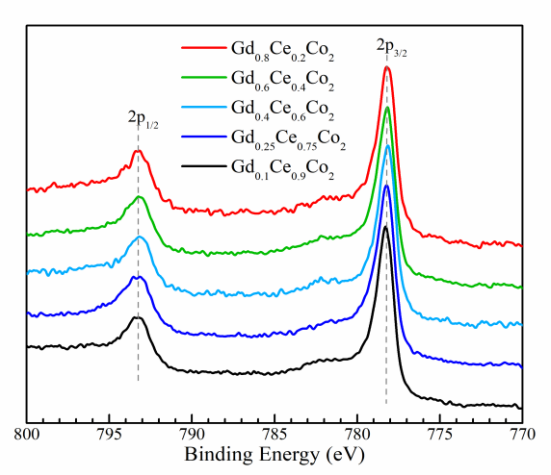

Figure 4.6. Co 2p XPS spectra of $Gd_{1-x}Ce_xCo_2$ compounds [46]

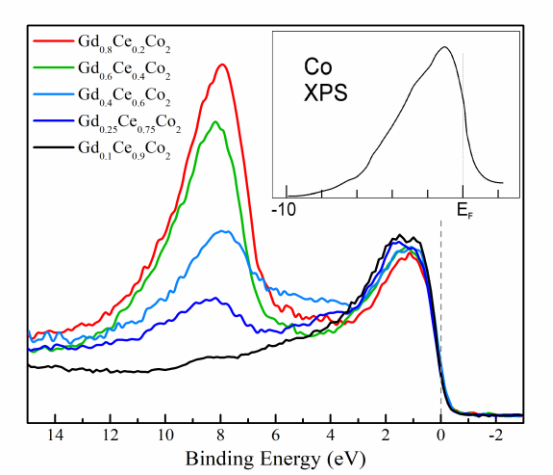

Figure 4.7. XPS valence band spectra of $Gd_{1-x}Ce_xCo_2$ compounds

4.3. Magnetic properties and magnetocaloric effect of $Gd_{1-x}Ce_xCo_2$ intemetallic compounds

The measured Zero Field Cooled (ZFC) – Field Cooled (FC) mode under a small applied magnetic field of 0.05 T show a bifurcation different behavior at low temperature for the investigated samples, **Figure 4.8**. The bifurcation temperature is increasing with Ce content, which could be related to the magnitude of magnetocrystalline anisotropies as a function of composition.

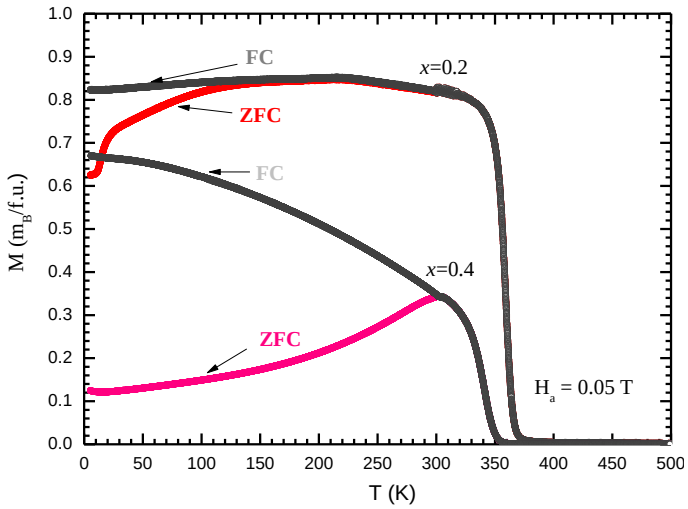

Figure 4.8. ZFCFC for $Gd_{1-x}Ce_xCo_2$ for x= 0.2, 0.4

The first magnetization derivatives of temperature were calculated in order to obtain the Curie temperature for all compounds, listed in **Table 4.1**. It can be observed that for the samples with a small Ce content (x = 0.1, 0.15,0.2, 0.25 and 0.3) the Curie temperature remains almost unchanged, around 360 K, due to the strong and dominate 3*d*-3*d* interaction. Increasing Ce content (x = 0.4, 0.5, 0.6, 0.75, 0.8), the distance Co – Co atoms increase, so a slight decrease in Curie temperature occurs, from 349 K to 275 K. Furthermore, if the cerium content is increased, for x = 0.9, the Curie temperature drops suddenly at 87 K. The substitution of Gd for Ce modifies the contributions associated with hybridization of 5d orbitals of Gd and 3d orbitals of Co, which leads to a reduction in Tc. From the magnetization isotherms recorded at 4.5 K in the applied magnetic fields up to 12 T result a similar behavior for $Gd_{1-x}Ce_xCo_2$ compounds, saturation being already reached in an applied magnetic field of 1 T, **Figure 4.9.**

The magnitude of the saturation magnetization decrease with the increase of Ce content, from a value about 4.12 μ_B/f.u for x = 0.2 to 1.03 μ_B/f.u for x = 0.8. This tendency is typical for ferrimagnetic order, the magnetic coupling between Gd moment and Co moment is antiparallelly oriented.

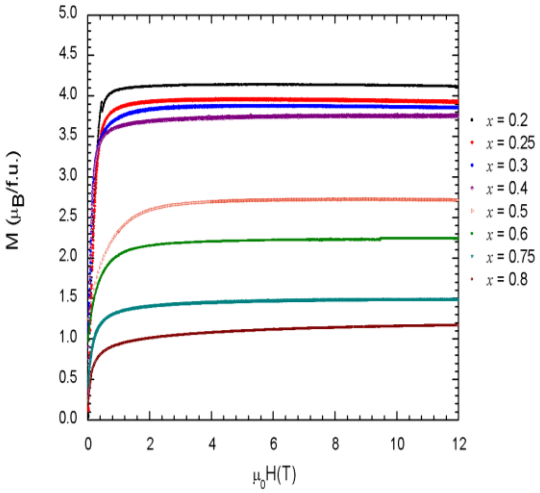

Figure 4.9. Magnetization isotherms for $Gd_{1-x}Ce_xCo_2$ at T = 4.5K, measured in an applied magnetic field up to 12 T

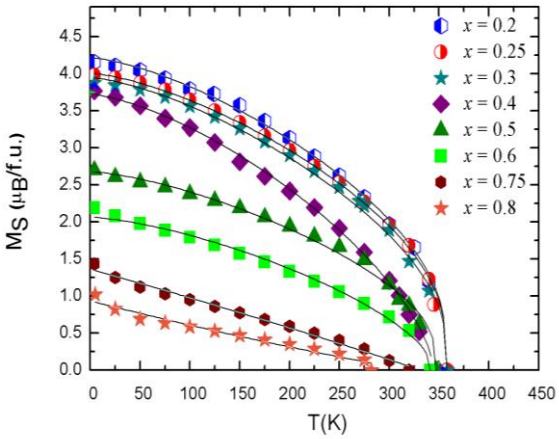

Figure 4.10. The temperature dependence of the saturation magnetization for $Gd_{1-x}Ce_xCo_2$ compounds

The spontaneous magnetization, Ms, for all investigated samples was determined from the measured magnetization isotherms using the approach to saturation law. The value of the spontaneous magnetization at 0 K is decreasing with the increase of Ce content from 4.56 μ_B/f.u for x = 0.1 to 1.03 μ_B/f.u for x = 0.8, as presented in **Table 4.1**, confirming the ferrimagnetically order in the investigated compounds. In order to estimate the magnetic moment for cobalt atoms in our specimens, a value of -0.75 μ_B/atom for Ce magnetic moment [32] and a value of 7.2 μ_B/atom [57] for Gd magnetic moment were considered. It can be observed that the obtained values for Co magnetic moment is dependent of cerium concentration, having a decreasing trend as the cerium concentration is increasing.

Table 4.1. The values of the Curie temperature, spontaneous magnetization at 0 K, and magnetic moments in $Gd_{1-x}Ce_xCo_2$ compounds

x	T_C (K)	M_0 (μ_B/f.u)	m_{Gd} (μ_B/atom)	m_{Ce} (μ_B/atom)	m_{Co} (μ_B/atom)
0.1	362	4.56	-7.2	-0.75	0.99
0.15	360	4.30	-7.2	-0.75	0.96
0.2	360	4.14	-7.2	-0.75	0.88
0.25	358	3.97	-7.2	-0.75	0.81
0.3	358	3.88	-7.2	-0.75	0.69
0.4	349	3.72	-7.2	-0.75	0.45
0.5	346	2.69	-7.2	-0.75	0.64
0.6	340	2.19	-7.2	-0.75	0.57
0.75	326	1.43	-7.2	-0.75	0.47
0.8	275	1.03	-7.2	-0.75	0.51

Based on the magnetization isotherms, measured between 280 K and 400 K with an increment of 5 K between measured magnetization isotherms, the magnetic entropy changes were calculated for $Gd_{1-x}Ce_xCo_2$ intermetallic compound with x = 0.2, 0.25, 0.3, 0.4, 0.5, 0.6 and 0.75. The temperature

dependences of magnetic entropy change in 2 T and 4 T external applied fields for $Gd_{1-x}Ce_xCo_2$ compounds are plotted in **Figure 4.11.**

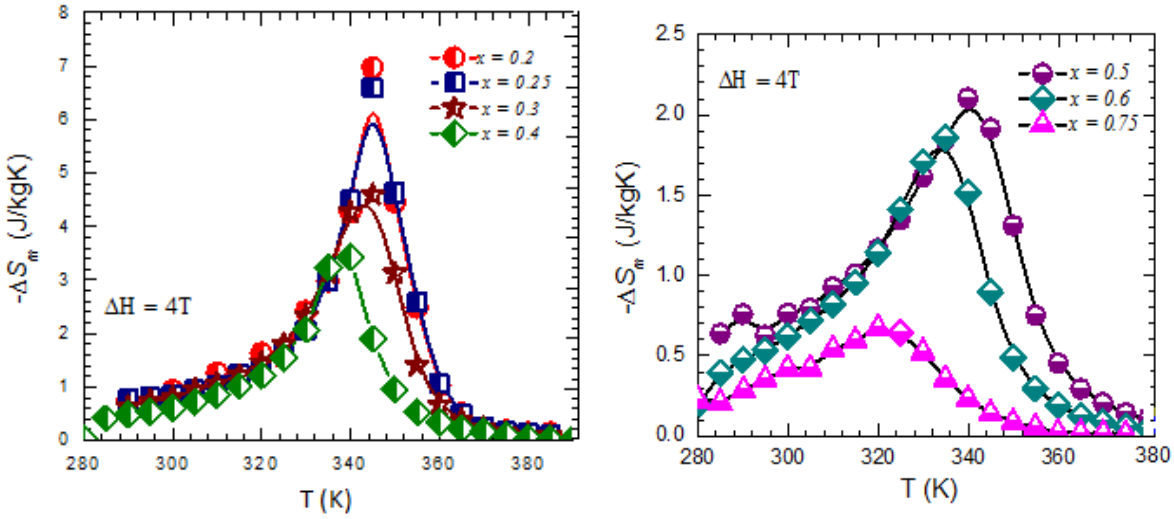

Figure 4.11. Magnetic entropy changes for $Gd_{1-x}Ce_xCo_2$ compounds

The maximum values of entropy change occur almost around the transition temperatures for all the compounds, **Table 4.2**. The second order magnetic phase transition is confirmed again by the approximate symmetry of the variation of magnetic entropy change around the Curie temperature. The magnetic entropy change decreases with the increase of cerium content, from 6.92 J/KgK for x = 0.2 to 0.66 J/KgK for x = 0.75 in the applied magnetic field of 4 T. The peak on the $\Delta S_M(T)$ curve in these compounds is broad, full width at half maximum is increasing with cerium concentration, having a maximum value of 42 K for x = 0.75. Therefore, the relative cooling power $RCP(S)$ which is calculated as a product between ΔS_M and δT_{FWHM} has small values, but not negligible, meaning that the investigated compounds display a moderate magnetocaloric effect. Also, the normalized cooling power to the applied magnetic field was calculated, showing small differences with the change of the applied magnetic field, and, therefore confirming the applicability of these compounds in the technological field.

Table 4.2. The maximum value of temperature, the maximum value of magnetic entropy change, the calculated relative cooling power parameter and the normalized cooling power to the applied magnetic field for $Gd_{1-x}Ce_xCo_2$ intermetallic compounds in an applied magnetic field of 4T

x	T_{max} (K)	$\lvert\Delta S_M\rvert$ (J/KgK)	δT_{FWHM} (K)	$RCP(S)$ (J/kg)	$RCP(S)/\Delta B$ (J/kgT)
0.2	344	6.92	17	117.64	29.41
0.25	345	6.53	19	124.07	31.02
0.3	344	4.49	23	103.27	25.81
0.4	340	2.08	37	76.96	19.24
0.5	337	3.42	18	61.59	15.39
0.6	333	1.79	33	59.07	14.77
0.75	320	0.66	43	28.38	7.09

Chapter 5

Electronic structure and magnetic behaviour of $GdCo_{2-x}A_x$ intermetallic compounds

In this chapter is presented a detailed correlated study of structural, electronic, and magnetic properties of $GdCo_{2-x}A_x$ Laves phase intermetallic compounds, where *A* = Ni, Mn, Cu and Al. To get a deep insight on the physical properties of the transition metal, different analysis tools have been combined: magnetic measurements, X-ray photoelectron spectroscopy (XPS) and band structure calculations. In view of potential applications in magnetic refrigeration, a full evaluation of magnetocaloric properties was accomplished for the compounds with substitutional *A* = Ni, Cu and Al.

5.1. Crystalographic analysis of $GdCo_{2-x}A_x$ intemetallic compounds

$GdCo_{2-x}Ni_x$ (x = 0.2, 0.25 and 0.3), $GdCo_{1.8}Al_{0.2}$ and $GdCo_{1.8}Cu_{0.2}$ were prepared by melting high purity (99.99%) ingots in an arc furnace under purified argon atmosphere. Their homogeneity was ensured by several times consecutive melting. The induction melting technique was used in order to prepare $GdCo_{2-x}Mn_x$ with *x = 0.1, 0.2* and *0.3* from high purity of Gd (99.9%), Co (99%), and Mn (99.99%) elements, under an argon atmosphere. All samples were thermally treated in vacuum at 850 ^oC for 7 days and slowly cooled to room temperature. X-ray diffraction (XRD) was recorded at room temperature on powder sample, using a Bruker D8 Advance AXS diffractometer with Cu Kα radiation.

The crystal structure and the lattice parameters were calculated by performing Rietveld refinements on the experimental XRD data using the FullProf suite [31]. In all cases only one phase was found, having the cubic $MgCu_2$ - Laves type structure. The Gd atoms occupies -43m sites while Co and *A* (*A*=Ni, Mn, Cu, Al) are distributed randomly in -3m positions. The calculated lattice parameters are presented in **Table 5.1.**

Table 5.1. *Lattice constants for $GdCo_{2-x}Mn_x$ compounds*

A	***x***	***a[Å]***
Ni	0.2	7.24(9)
	0.25	7.24(7)
	0.3	7.24(4)
Mn	0.1	7.27(4)
	0.2	7.29(6)
	0.3	7.31(8)
Cu	0.2	7.27(8)
Al	0.2	7.31(2)

The change in lattice parameter is almost negligible when Co is substituted by Ni, which is somewhat expected, considering the close values of atomic radii for cobalt (125 pm) and nickel (124 pm). For $GdCo_{2-x}Mn_x$ compounds the lattice constant, calculated from Rietveld refinement, increases as the manganese content increases, as expected, considering the atomic radius of manganese (140 pm) larger than that of cobalt (125 pm). The lattice parameter of $GdCo_{1.8}Cu_{0.2}$ is smaller that of $GdCo_{1.8}Al_{0.2}$ compound due to the smaller atomic radius of Cu (128 pm) compared with Al (143 pm) atomic radius.

5.2. Band structure calculations and electronic structure of $GdCo_{1.8}A_{0.2}$ intemetallic compounds

Using the FP-LAPW Wien2k computational code, to describe the $GdCo_{1.8}A_{0.2}$ cubic Laves phase (C15) systems, a supercell model has been used. From the *ab-initio* calculations we can conclude that the ground state of the system corresponds to an antiferromagnetic alignment of the spin magnetic moments of Gd and Co atoms, the total energy for the antiferromagnetic state being about 0.11Ry lower than the ferromagnetic state.

Considering the calculated total magnetic moment in the interstitial zone of 3.80 μ_B, the total magnetic moment per formula unit for the $GdCo_{1.8}Ni_{0.2}$ compound was found to be 5.52 μ_B. This value is slightly larger but in good agreement with the experimental value of 5.38 μ_B (see **Table 5.2.**). The total magnetic moment obtained for $GdCo_{1.8}Mn_{0.2}$ specimen is 4.48 μ_B/f.u., in the intestitial zone of 3.87 μ_B, very close to the 4.51 μ_B/f.u.value obtained from magnetic measurements and the average calculated magnetic moment for manganese is 2.86 μ_B. Also, the computed and experimental results are in very good agreement for the total magnetic moment per formula unit of $GdCo_{1.8}Al_{0.2}$ and $GdCo_{1.8}Cu_{0.2}$ compounds, being 5.80 μ_B/f.u for $GdCo_{1.8}Al_{0.2}$and 6.03 μ_B/f.u for $GdCo_{1.8}Cu_{0.2}$ (calculated) and 5.78 μ_B/f.u for $GdCo_{1.8}Al_{0.2}$ and 5.75 μ_B/f.u for $GdCo_{1.8}Cu_{0.2}$ (experimental). As reference, we also calculated the electronic properties of the $GdCo_2$ compound, for which the total magnetic moment per formula unit was found to be smaller (5.17 μ_B).

Table 5.2. *The computed magnetic moments of $GdCo_{1.8}A_{0.2}$ compounds*

Atom	*Position*	*Spin moment* (μ_B) *A*=Ni	*Spin moment* (μ_B) *A*=Mn	*Spin moment* (μ_B) *A* = Cu	*Spin moment* (μ_B) *A* = Al
Gd1	(1/8, 1/8,1/8)	7.27	7.28	7.27	7.27
Gd2	(7/8,7/8,7/8)	7.26	7.30	7.27	7.25
Gd3	(5/8, 5/8, 1/8)	7.26	7.30	7.27	7.26
Gd4	(3/8,3/8,7/8)	7.26	7.30	7.27	7.26
Gd5	(5/8,1/8,5/8)	7.26	7.30	7.27	7.26
Gd6	(3/8,7/8,3/8)	7.26	7.30	7.27	7.26
Gd7	(1/8,5/8,5/8)	7.26	7.30	7.27	7.25
Gd8	(7/8, 3/8,3/8)	7.27	7.28	7.27	7.27
A	(1/2,1/2,1/2)	-0.29	-2.88	0.02	0.03
A	(1/2,3/4,3/4)	-0.29	-2.81	0.03	0.02
Co3	(3/4,3/4,1/2)	-1.27	-1.34	-1.15	-0.90
Co4	(3/4,1/2,3/4)	-1.27	-1.34	-1.15	-0.90
Co5	(0,0,1/2)	-1.29	-1.41	-1.20	-1.18
Co6	(0,1/4,3/4)	-1.33	-1.40	-1.29	-1.18
Co7	(1/4,1/4,1/2)	-1.32	-1.36	-1.25	-1.09
Co8	(1/4,0,3/4)	-1.27	-1.34	-1.15	-0.90
Co9	(0,1/2,0)	-1.29	-1.41	-1.20	-1.18
Co10	(0,3/4,1/4)	-1.33	-1.40	-1.29	-1.18
Co11	(1/4,3/4,0)	-1.27	-1.34	-1.15	-0.90
Co12	(1/4,1/2,1/4)	-1.32	-1.36	-1.25	-1.09
A	(1/2,0,0)	-0.29	-2.88	0.02	0.03
Co14	(1/2,1/4,1/4)	-1.27	-1.38	-1.23	-1.02
Co15	(3/4,1/4,0)	-1.32	-1.36	-1.25	-1.09
Co16	(3/4,0,1/2)	-1.32	-1.36	-1.25	-1.09

The band structure analysis allows us to get deeper in the mechanisms responsible on the magnetic moments of each element in the compounds. First, a larger calculated Gd moments with respect to the atomic expectation (7 μ_B) clearly comes from the hybridization of the Gd-5*d* and Co-3*d* orbitals: from the spin resolved valence charge distribution analysis we extract exactly the additional 0.26 μ_B contribution of the hybrid 5*d*-Gd orbital to the total Gd spin magnetic moment. The coupling between Gd and the transition metals is therefore mediated by the 5*d* electrons of Gd hybridized with the 3*d* electrons of the transition metal (Co, Ni). Second, the $GdCo_{1.8}Ni_{0.2}$ density of states analysis reveals the main mechanisms responsible of the reduction of the spin magnetic moment of Co when doping with Ni. They are mainly related to Co-Ni hybridization and not simply to a rigid band energy downward displacement effect, due to the extra-electron brought by the substitutional doping Ni in the Co host places.

5.3. XPS spectra of $GdCo_{2-x}A_x$ intemetallic compounds

XPS core level spectra provide important information on the electronic structure, especially in the case of 3*d* transition metal ions. The multiplet splitting of the 3*s* line for 3*d* transition metals with a local magnetic moment is a good measure of the local moment of the ground state only when the charge–transfer satellite in the 2*p* core level spectra is small.

5.3.1 XPS spectra of $GdCo_{2-x}Ni_x$ intemetallic compounds

The Co 2p XPS spectra (**Figure 5.1**) are dominated by two features located at 778.2 eV and 793.2 eV attributed to the $2p_{3/2}$ and $2p_{1/2}$ states. Both these states are accompanied by broad satellite lines at higher binding energies, which may be explained by assuming more than one $3d^n$ final state configuration.

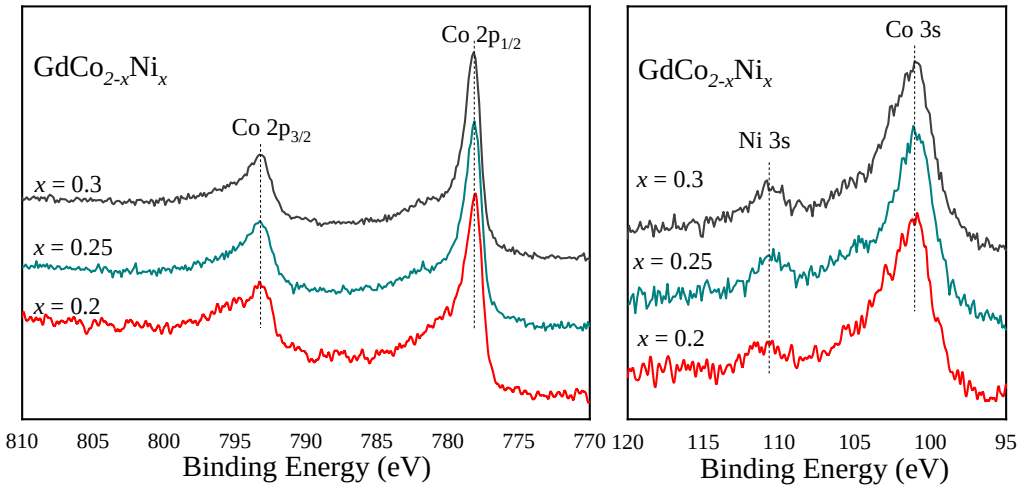

Figure 5.1. Co 2p (right) and Co 3s (left) XPS spectra of $GdCo_{2-x}Ni_x$ compounds

The Co 3s core level spectra show a main line located at about 101 eV and a satellite at higher binding energy, due to the exchange interaction J_{dc} between the core hole spin *s* and the 3*d* electron spin S in all investigated compounds. [8]. In order to evaluate the exchange splitting, the XPS spectra were fitted in the 90 eV to 120 eV binding energy region using three components: two Co 3*s* peaks, corresponding to the high spin final sate S +1/2 and the low spin final state S-1/2, respectively, and one for the Ni 3*s* core level, which is situated at about 110.7 eV. For all investigated samples we found an

exchange splitting of about 3.2 eV between the high spin final state and the low spin final state of the Co 3*s* core level, smaller to that found in the pure Co metal, namely 4.5 eV [55]. Since the exchange splitting $\Delta E_{ex} = J_{dc}(2S + 1)$ is proportional with the Co local moment [58], we estimate an average magnetic moment for Co ions of about 1.2 μ_B in all investigated $GdCo_{2-x}Ni_x$ compounds.

The XPS valence band spectra of $GdCo_{2-x}Ni_x$ compounds are presented in **Figure 5.2.** The centroids near Fermi level, located at 1.15 eV are assigned to Co 3*d* states, a value very close to that observed in Co metal. The presence of the intense peaks observed at 8.1 eV is the contribution from Gd 4*f* state.

5.3.2 XPS spectra of $GdCo_{2-x}Mn_x$ intemetallic compounds

The valence band XPS spectra for $GdCo_{1.8}Mn_{0.2}$ compound, **Figure 5.3**. is dominated by the Co 3*d* states situated at about 1.1 eV. The Mn 3*d* states are situated in the 2.5 – 3 eV region of the valence band. The contribution of Gd 4*f* is localized at 8.1 eV, like previously shown for $GdCo_{2-x}Ni_x$.

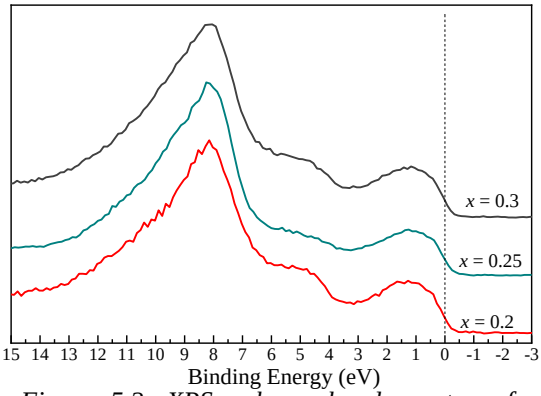

Figure 5.2. XPS valence band spectra of $GdCo_{2-x}Ni_x$

The line-shape analysis of the XPS spectra in the 85 eV to 120 eV binding energy region, shown in **Figure 5.4** for $GdCo_{1.8}Mn_{0.2}$, reveals the exchange splitting of both the Co 3*s* and Mn 3*s* core levels, which is direct evidence of the local magnetic moments on both Co and Mn sites. In order to evaluate the exchange splitting in $GdCo_{1.8}Mn_{0.2}$ compound, the XPS spectra in the 85 eV to 120 eV binding energy region was fitted after the subtraction of a Shirley type background. The Co 3*s* XPS spectrum shows an exchange splitting of about 3.5 eV, smaller than that found in the pure Co metal, namely 4.5 eV, but close to the value found for $GdCo_{2-x}Ni_x$ compounds. The Mn 3*s* core level spectra shows an exchange splitting around 2.7 eV, indicating a magnetic moment of about 2 μ_B/Mn, considering that a magnetic moment of 4 μ_B /Mn produces an exchange splitting of 5.2 eV in MnNi.

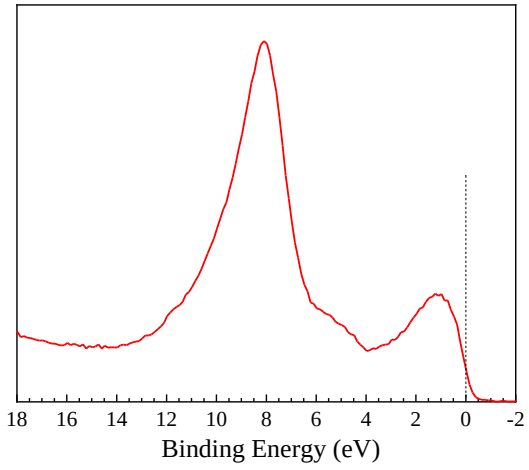

Figure 5.3. XPS valence band spectra of $GdCo_{1.8}Mn_{0.2}$

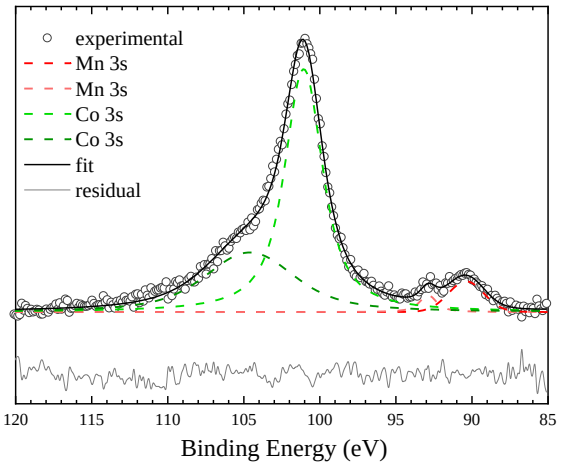

Figure 5.4. XPS spectrum of Co3s and Mn 3s core levels in $GdCo_{1.8}Mn_{0.2}$ compound

5.3.3 XPS spectra of $GdCo_{1.8}Cu_{0.2}$ and $GdCo_{1.8}Al_{0.2}$ intemetallic compounds

The XPS valence band spectra for investigated compounds are presented in Figure 5.14. The high intensity peaks located at 8.2 eV for $GdCo_{1.8}Al_{0.2}$ compound and 8.1 eV for $GdCo_{1.8}Cu_{0.2}$ are due to the Gd 4*f* states. The Cu 3*d* states are centered at about 3.7 eV, as clearly seen in the spectra of $GdCo_{1.8}Cu_{0.2}$. The noticeable difference between the two spectra, at binding energy below 3 eV, is due to the Al 3*s* and Al 3*p* states, which are located close to the Fermi level.

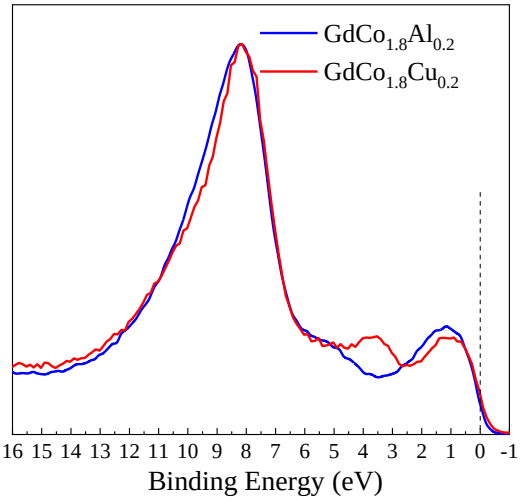

Figure 5.5. XPS valence band for $GdCo_{1.8}Al_{0.2}$ and $GdCo_{1.8}Cu_{0.2}$ compounds

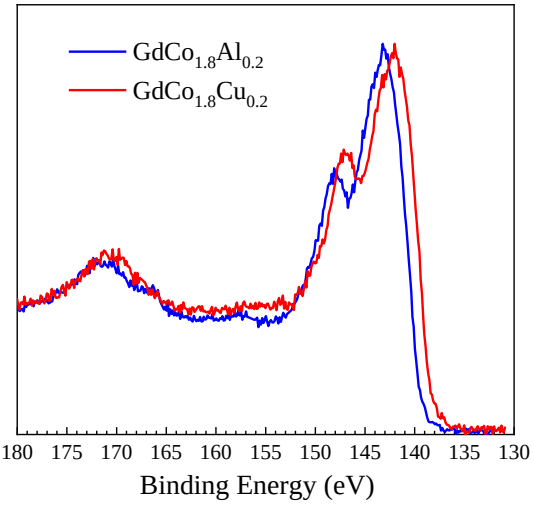

Figure 5.6. Gd 4d XPS spectra for $GdCo_{1.8}Al_{0.2}$ and $GdCo_{1.8}Cu_{0.2}$ compounds

Gd 4*d* XPS spectra for $GdCo_{1.8}Al_{0.2}$ and $GdCo_{1.8}Cu_{0.2}$ compounds spectra is presented in **Figure 5.6.** A shift in the Gd 4*d* peaks position towards higher binding energy is observed upon on substitution of Co by Cu/Al compared to previously investigated $GdCo_{1.8}Mn_{0.2}$ and $GdCo_{2-x}Ni_x$ compounds, which can be attributed to the charge transfer from Gd to neighboring atoms.

The Co 3*s* XPS spectra for the investigated compounds are very similar, as illustrated in **Figure 5.7.**

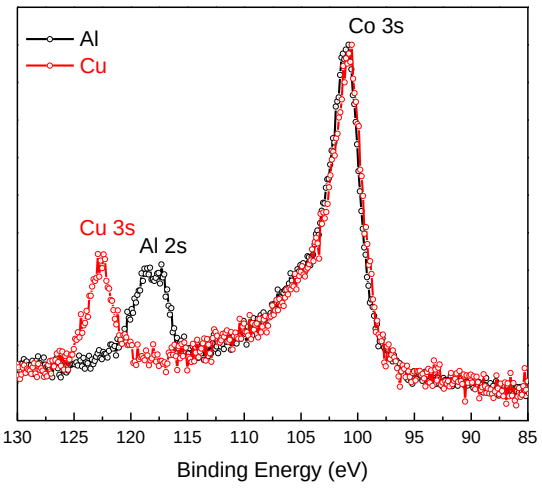

Figure 5.7. XPS spectra of $GdCo_{1.8}Al_{0.2}$ and $GdCo_{1.8}Cu_{0.2}$ compounds

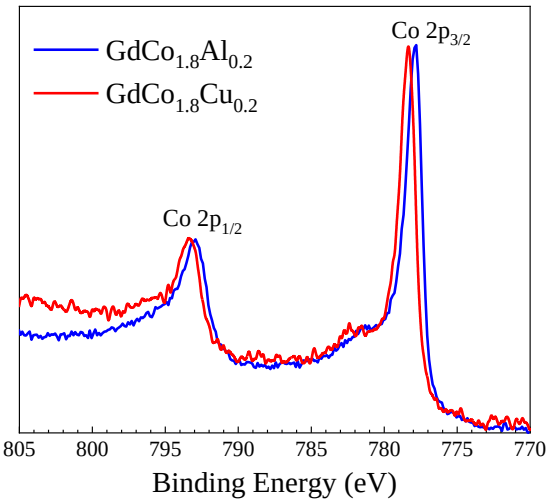

Figure 5.8. Co 2p XPS spectra of $GdCo_{1.8}Al_{0.2}$ and $GdCo_{1.8}Cu_{0.2}$ compounds

For both samples, the Co 3*s* core level spectra show an exchange splitting, arising from the exchange interactions between the core hole and open 3*d* shell. The Al 2*s* states in $GdCo_{1.8}Al_{0.2}$ and Cu 3*s* states in $GdCo_{1.8}Cu_{0.2}$ are located at higher binding energy, at 118.2 eV and 122.6 eV, respectively. After fitting the XPS spectra in the 90 eV to 130 eV binding energy region, the values obtained for the exchange splitting ΔE_{ex}, which are proportional with the Co local moment, were used to estimate an average magnetic of about 1.3 μ_B for the Co ions in both $GdCo_{1.8}Al_{0.2}$ and $GdCo_{1.8}Cu_{0.2}$ compounds.. The Co 2*p* XPS spectra for the investigated $GdCo_{1.8}Al_{0.2}$ and $GdCo_{1.8}Cu_{0.2}$ compounds are presented in Figure 5.18. The Co 2*p* XPS for both $GdCo_{1.8}Al_{0.2}$ and $GdCo_{1.8}Cu_{0.2}$ compounds present a spin-orbit splitting of about 15 eV. The position of the Co $2p_{3/2}$ and $2p_{1/2}$ peaks in the XPS spectra of $GdCo_{1.8}Cu_{0.2}$ is very close to the ones previously presented for $GdCo_{1.8}Mn_{0.2}$ and $GdCo_{2-x}Ni_x$ compounds. The shift to lower binding energies of the Co 2*p* core level spectra of $GdCo_{1.8}Al_{0.2}$ is due to the increase of interatomic distances, as the lattice parameter is larger than for the other investigated $GdCo_{1.8}A_{0.2}$ compounds.

5.4. Magnetic properties of $GdCo_{2-x}A_x$ intemetallic compounds

5.4.1. Magnetic properties of $GdCo_{2-x}Ni_x$ intemetallic compounds

The magnetization measurements as a function of temperature, in the applied magnetic field of 0.05T are presented in **Figure 5.9**. indicate that all the prepared compounds undergo a transition from the paramagnetic state to the ordered magnetic state. The Curie temperatures were calculated as the minima in the first derivative of magnetization dM/dT vs temperature and plotted in the inset of **Figure 5.9.** As the concentration of Ni increases, the Curie temperature, T_C, significantly gets reduced towards room temperature as can be seen in **Table 5.3.** The Curie temperature is determined, mainly, by the *M*-*M* strength interaction which depends both on the interatomic distances and the number of nearest neighbors [59]. In our case the substitution of Co by Ni modifies the exchange Co3*d* - Co3*d* interactions (Co3*d* - Ni3*d* or Ni3*d* - Ni3*d* being weaker), enabling the decrease of T_C toward room temperature. Therefore, the almost inversely proportional decrease of Curie temperature on Ni concentration value can be attributed to the magnetic dilution.

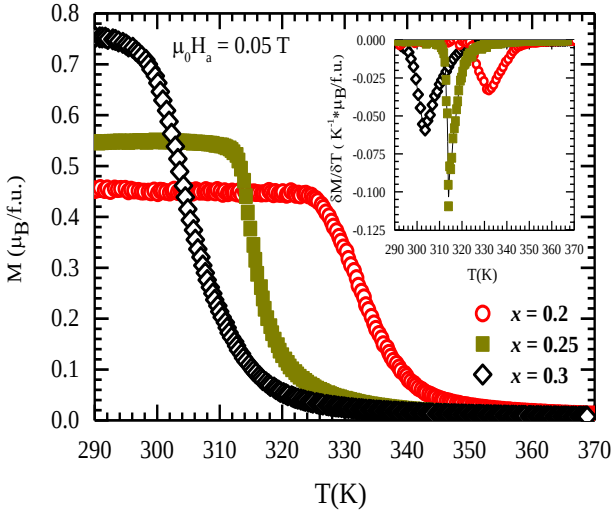

Figure 5.9. The magnetization vs temperature for $GdCo_{2-x}Ni_x$ compounds, in the applied magnetic field of 0.05T. The inset shows the first derivative of magnetization vs temperature.

The magnetization isotherms recorded at 4.2 K are plotted in **Figure 5.10.** Values of 4.96 μ_B/f.u [60], 5 μ_B/f.u [61] 4.89 μ_B/f.u [62] were reported previously for the saturation magnetization in the parent compound, $GdCo_2$. The saturation magnetization values obtained for $GdCo_{2-x}Ni_x$ compounds increases when replacing cobalt by nickel is in good agreement with a ferrimagnetic-type ordering, gadolinium and cobalt magnetic moments being antiparallelly oriented.

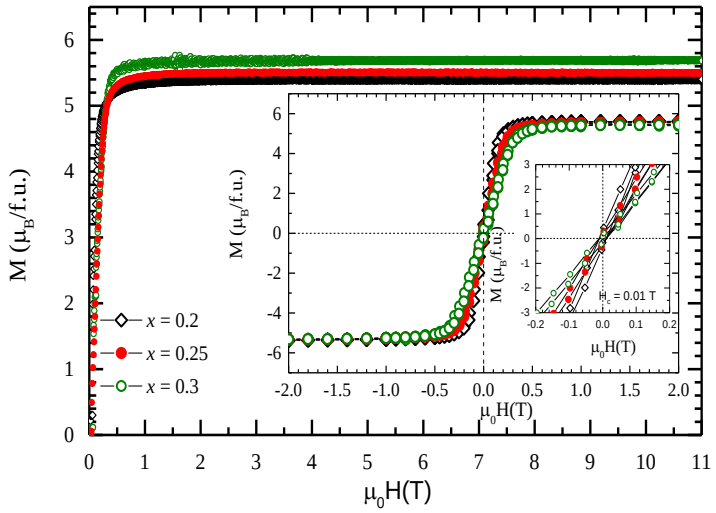

Figure 5.10. Magnetic isotherms of $GdCo_{2-x}Ni_x$ compounds at 4.2 K in the applied magnetic field up to 10 T. The inset shows the magnetic hysteresis for the investigated samples at 4.2 K.

Table 5.3. *The values of the Curie temperature, saturation magnetization, and magnetic moments in $GdCo_{2-x}Ni_x$ compounds. The values of 7.26 μ_B for Gd moment and -0.29 μ_B for Ni moment were extracted from from ab-initio calculations -see section 5.2.*

x	*Tc (K)*	*M_0 (μ_B/f.u.)*	*m_{Gd} (μ_B/atom)*	*m_{Ni} (μ_B/atom)*	*m_{Co} (μ_B/atom)*
0.2	332	5.38	7.26	-0.29	-1.01
0.25	313	5.50	7.26	-0.29	-0.96
0.3	303	5.68	7.26	-0.29	-0.88

The substitution of Co by Ni modifies the strength of 3*d*-3*d* exchange interactions, being smaller in Co 3*d*-Ni 3*d* than in Co 3*d*-Co 3*d*. This roughly explains the decrease of the Curie temperature when substituting the Co with Ni. Moreover, the Ni substitution slightly lowers the Co magnetic moment in $GdCo_{2-x}Ni_x$ compounds. The mechanisms of the cobalt magnetic moment decrease are deeper revealed by band structure analysis (see section 5.2). It is mainly related to Co-Ni hybridization and filling of bands with extra-electrons provided by Ni that has one more electron with respect to Co.

5.4.2. Magnetic properties of $GdCo_{2-x}Mn_x$ intemetallic compounds

Magnetic measurements for the $GdCo_{2-x}Mn_x$ were performed in a wide temperature range, 4K – 550 K and the applied magnetic field used for investigations was up to 12 T. Zero Field Cooled (ZFC) – Field Cooled (FC) magnetizations curves, recorded under a small applied magnetic field of 0.05T, are plotted as a function of temperature in **Figure 5.11,** for $GdCo_{1.8}Mn_{0.2}$ sample. The separation of ZFC and FC magnetization curves below 270 K is a signature of spin glass like behavior, which could be explained by the existence of random distribution of the magnetic ions or magnetocrystalline anisotropy which is related to the magnitude of coercivity at low temperature.

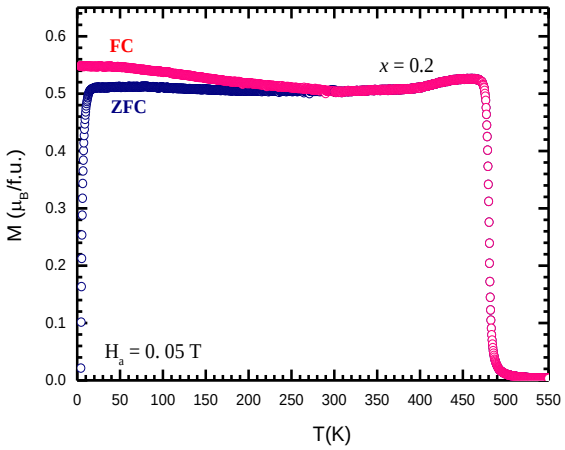

Figure 5.11. Curves showing Zero Field Cooled (ZFC) – Field Cooled (FC) for $GdCo_{1.8}Mn_{0.2}$ sample

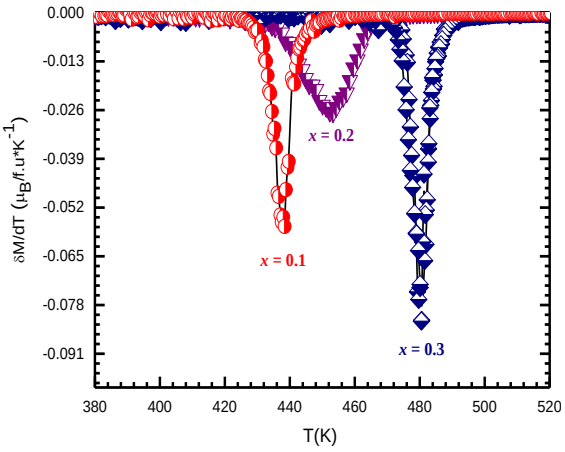

Figure 5.12. The derivative of the magnetizations versus temperature for $GdCo_{2-x}Mn_x$ compounds

The temperature dependences of magnetizations for the samples with x = 0.1 and x = 0.3 were also recorded in small applied magnetic field of 0.05 T, with the purpose of obtaining the Curie temperatures. Thus, the first derivative of magnetization as temperature were calculated and plotted in **Figure 5.12.** An increase of the transition temperatures with the manganese content were observed from 436 K for x = 0.1 to 479 K for x = 0.3, listed in **Table 5.4.**

Investigated samples were subjected to the 12 T applied magnetic field in order to record the magnetization isotherms at a temperature of 4 K. It can be noticed a downward trend for the saturation magnetization as the manganese content is higher, 4.89 μ_B/f.u. for x = 0.1, 4.51 μ_B/f.u. for x = 0.2 and 4.22 μ_B/f.u. for x = 0.3. This trend is typically for ferrimagnetically ordered systems with an antiparallel orientation of Gd and Co/Mn magnetic moments. Considering this, and the upper results obtained from band structure calculations which established a value of 7.29 μ_B/atom for gadolinium magnetic moment and 2.86 μ_B/atom for manganese magnetic moment (see Table 5.2) we have calculated the magnetic moments for cobalt atoms. The results are listed in **Table 5.4** and show an increase of cobalt magnetic moment with the manganese content, from 1.11 μ_B/at. for x = 0.1 to 1.30 μ_B/at. for x = 0.3.

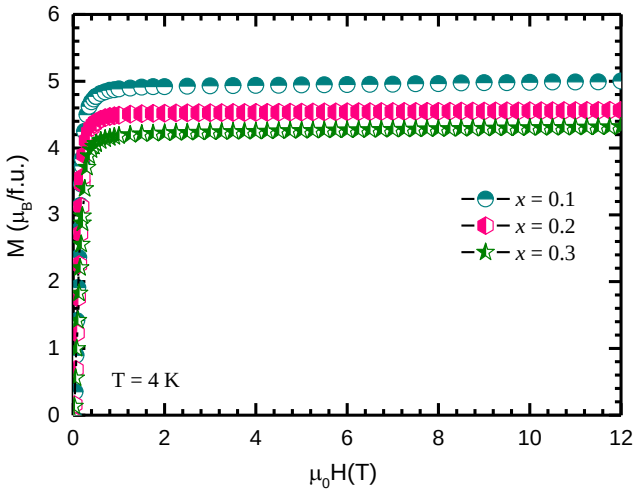

Figure 5.13. The magnetization isotherms measured in external magnetic field up to 12 T at 4 K

Table 5.4. *Curie temperatures for $GdCo_{2-x}Mn_x$, saturation magnetization at 4K, reported magnetic moment for Gd and Mn, calculated magnetic moment for Co*

x	T_c (K)	M_s (μ_B/f.u.)	m_{Gd} (μ_B/atom)	m_{Mn} (μ_B/atom)	m_{Co} (μ_B/atom)
0.1	436	4.89	7.29	-2.86	-1.11
0.2	452	4.51	7.29	-2.86	-1.22
0.3	479	4.22	7.29	-2.86	-1.30

5.4.1. Magnetic properties of $GdCo_{1.8}Cu_{0.2}$ and $GdCo_{1.8}Al_{0.2}$ intemetallic compounds

The temperature dependence of the magnetization in a small applied magnetic field of 0.05 T was recorded for $GdCo_{1.8}Al_{0.2}$ and $GdCo_{1.8}Cu_{0.2}$ compounds in order to calculate the transition temperature. The Curie temperatures were determined as the minimum values of the first derivative of magnetization as a function of temperature, plotted in **Figure 5.14**, inset. The obtained values were 378 K for the sample doped with copper and 382 K for the aluminium one, very close to each other.

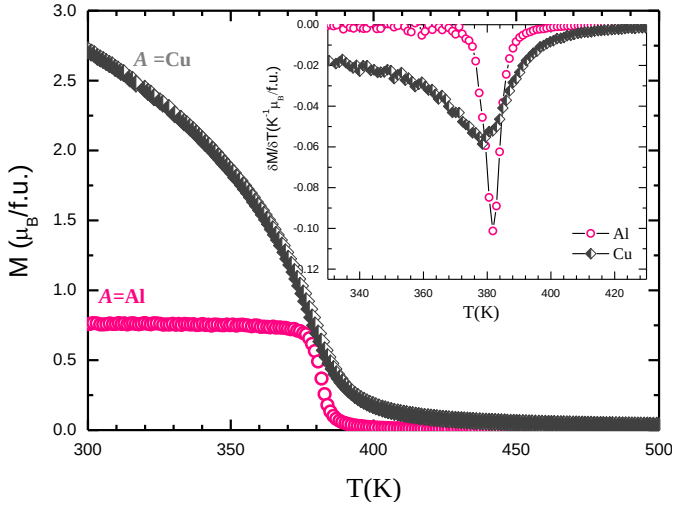

Figure 5.14. Magnetization versus temperature and the first derivative of magnetization as a function of temperature (inset) for $GdCo_{1.8}Al_{0.2}$ and $GdCo_{1.8}Cu_{0.2}$ compounds

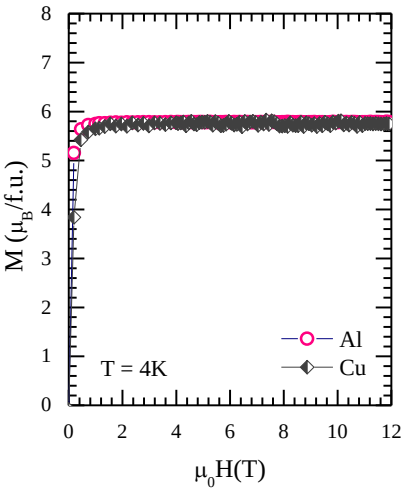

Figure 5.15. Magnetization isotherms at 4 K for $GdCo_{1.8}Al_{0.2}$ and $GdCo_{1.8}Cu_{0.2}$

From magnetization isotherms measured at 4 K in the applied magnetic field up to 8 T, the saturation magnetization has been calculated. The saturation magnetizations have very close values, 5.75 μ_B/f.u for the copper sample and 5.78 μ_B/f.u for the aluminium sample. Therefore, using the obtained magnetic moment from our band structure calculation 7.29 μ_B/atom for Gd, 0.2 μ_B/atom for Cu and 0.3 μ_B/atom for Al and considering an antiparallel alignment of Gd and Co/Cu, Al magnetic moments the cobalt magnetic moment has been estimated to be 0.83 μ_B/atom for copper sample and 0.81 μ_B/atom for aluminium sample. The decrease of the Co magnetic moment compared with undoped sample can be explained by weakening the 3*d*-3*d* exchange interactions due to substitution with almost non-magnetic Cu or Al.

5.5. Magnetocaloric effect of $GdCo_{2-x}A_x$ intemetallic compounds

5.5.1. Magnetocaloric effect of $GdCo_{2-x}Ni_x$ intermetallic compounds

The magnetic entropy change was calculated based on the magnetization isotherms measured between 280 K and 380 K, with a step of 5 K, in the external magnetic field between 0-2 T and respectively 0-4 T and plotted as a function of temperature in **Figure 5.16.** The substitution of Co by Ni causes a very small increase in maximum entropy change values, as listed in **Table 5.5**. Nevertheless, the $|\Delta S_m|$ peaks are broader, which is mandatory for a good refrigerant material.

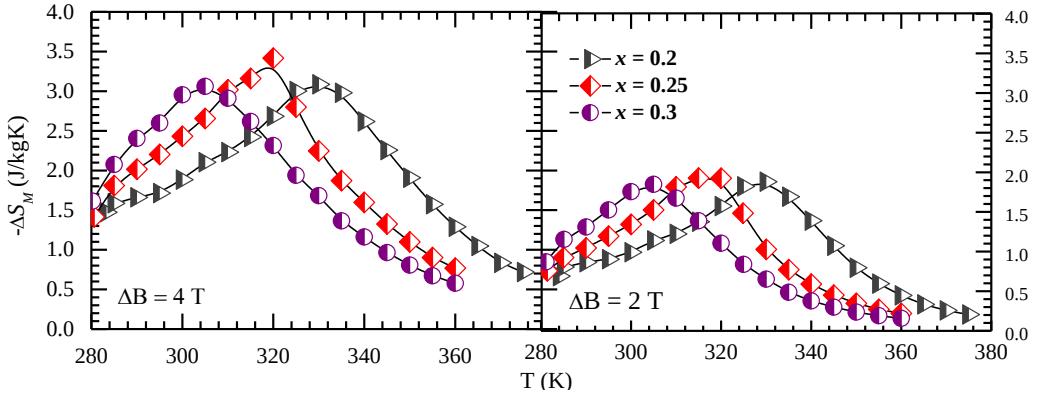

Figure 5.16. The temperature dependences of the magnetic entropy change for $GdCo_{2-x}Ni_x$

The magnetic refrigeration efficiency was evaluated by calculating the relative cooling power (*RCP*) for all the investigated samples, larger values corresponding to better magnetocaloric materials [58]. The *RCP(*ΔS*)* values, presented in **Table 5.5**, are rather large, indicating that the materials could be used for the magnetic refrigeration applications. For technical application it is better to use another characteristic parameter, related to the external field variation, namely the specific renormalized cooling power, *RCP*(Δ*S*)/Δ*B* (**Table 5.5**) [63]. For our samples *RCP*(Δ*S*)/Δ*B* values decreases slowly when the Ni concentration increases but do not depend significantly on the applied magnetic field change. The decrease of the *RCP*(Δ*S*)/Δ*B* values with increasing Ni concentration could be attributed to the narrowing of the $|\Delta S_m|$ peaks.

Table 5.5. *The magnetocaloric parameters for $GdCo_{2-x}Ni_x$ compounds*

x	**T_{max} (K)**	**$\|\Delta S_M\|$ (J/KgK)**		***δT*** $_{FWHM}$ **(K)**		***RCP*(Δ*S*) (J/kg)**		***RCP*(Δ*S*)/ΔB (J/kgT)**	
		ΔB=4T	ΔB=2T	ΔB=4T	ΔB=2T	ΔB=4T	ΔB=2T	ΔB=4T	ΔB=2T
0.2	330	3.07	1.82	71	55	217.97	100.10	54.49	50.05
0.25	319	3.43	2.00	59	46	202.37	92.00	50.59	46.00
0.3	304	3.07	1.84	46	44	141.22	80.96	35.30	40.48

5.5.2. Magnetocaloric effect of $GdCo_{1.8}Cu_{0.2}$ and $GdCo_{1.8}Al_{0.2}$ intermetallic compounds

The magnetic entropy changes were calculated for $GdCo_{1.8}Al_{0.2}$ and $GdCo_{1.8}Cu_{0.2}$ compounds from magnetization isotherms measured with a step of 5 K in the temperature range 320 K – 440 K. The maximum value of magnetic entropy change is reached at a temperature very close with the transition temperature for $GdCo_{1.8}Cu_{0.2}$ sample, being 381 K, while for $GdCo_{1.8}Al_{0.2}$ sample is reached at the same

temperature as the transition one, 382 K. As can be observed, the $|\Delta S_M|$ peaks are sensitive to the applied magnetic field, the maximum value of magnetic entropy changes is decreasing if the applied field is reduced from 4 T to 1 T.

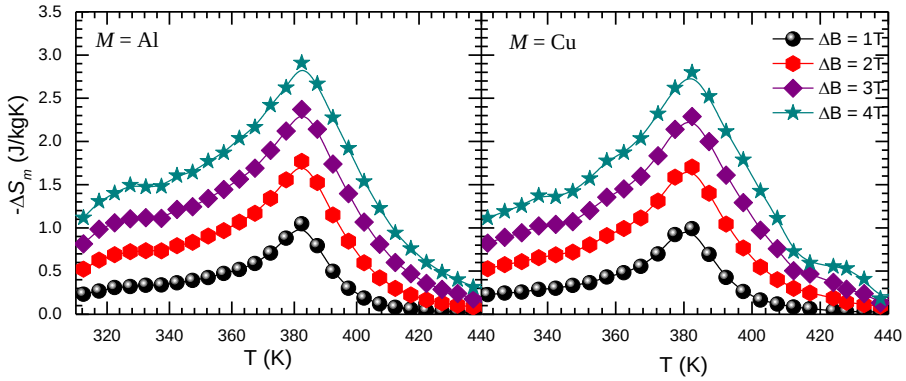

Figure 5.17. The temperature dependence of the magnetic entropy change for $GdCo_{1.8}Al_{0.2}$ (left) and $GdCo_{1.8}Cu_{0.2}$ (right) in an external magnetic field of 1 T, 2 T, 3 T and 4 T.

The substitution of Co for Cu or Al doesn't cause a significant change on the maximum value of magnetic entropy changes, see **Table 5.6.** The obtained values for normalized *RCP* at applied magnetic field are close to each other for both investigated compounds, making them suitable candidates for magnetic refrigerators materials.

Table 5.6. *The maximum value of temperature, the maximum value of magnetic entropy change,the calculated relative cooling power parameter (RCP) and the normalized RCP to the applied magnetic field for $GdCo_{1.8}Al_{0.2}$ and $GdCo_{1.8}Cu_{0.2}$ compounds*

A	T_{mx} (K)	$\|\Delta S_M\|$ (J/KgK)		δT_{FWHM} (K)		RCP(S) (J/kg)		RCP(S)/ΔB (J/kgT)	
		ΔB=2T	ΔB=4T	ΔB=2T	ΔB=4T	ΔB=2T	ΔB=4T	ΔB=2T	ΔB=4T
Cu	381	1.64	2.71	45	66	73.8	178.86	36.9	44.71
Al	382	1.76	2.89	48	82	84.48	236.98	42.24	59.24

Chapter 6
Conclusions

In this work we succeeded to point out some physical properties of RM_2 Laves phase type intermetallic compounds, additionally to the existing researches on this class of compounds. Arc melting technique was used for preparing $Ce_{1-x}Y_xFe_2$, $Gd_{1-x}Ce_xCo_2$, $GdCo_{2-x}A_x$ (A=Ni, Cu, Al) systems and induction technique for $GdCo_{2-x}A_x$ (A = Mn) systems, using high purity starting elements, and structural properties were investigated by X-ray diffraction measurements. The dopant concentration was chosen to adjust the transition temperature as close as possible to the room temperature. In order to get a deep understanding of the physical properties of the transition metal, different analysis instruments have been combined: magnetic measurements, X-ray photoelectron spectroscopy (XPS) and band structure calculations. A full evaluation of magnetocaloric properties was carried out in order to check the possibility to use the investigated systems in magnetic refrigeration field.

The prepared $Ce_{1-x}Y_xFe_2$ compounds with $x \leq 0.25$ are single phase with a cubic Laves phase type structure. The band structure calculations show an antiferomagnetic couupling of Fe magnetic moments to the Ce/Y ones. The computed magnetic moments for Fe atoms are in good agreement with the experimental ones. The magnetic measurements indicate that the samples are ferrimagnetically ordered with a second order magnetic phase transition and a roughly linear increase of the Curie temperature with Y concentration. A moderate magnetocaloric effect was found for all samples, with the maximum entropy change located at temperatures near the magnetic transition ones. Considering the possibility to tune the transition temperature and the magnetocaloric effect around room temperature, together with the high RCP(S) values, the broadened magnetic entropy curves and the absence of magnetic hysteresis, these materials are promising candidates for magnetic refrigeration devices.

The cubic Laves phase $Gd_{1-x}Ce_xCo_2$ compounds (x = 0.1, 0.15, 0.2, 0.25, 0.3, 0.4, 0.5, 0.6, 0.75, 0.8 and 0.9) were successfully prepared, structure analysis indicating that all the samples are single phase. The recorded XPS core level spectra show that Ce ions are in intermediate valence state and that the magnetic moments of Co atoms have almost the same magnitude in all compounds, but being smaller than in pure Co metal. The XPS valence band spectra of $Gd_{1-x}Ce_xCo_2$ compounds are mainly the result of the Co 3*d*, Ce 5*d*, and Ce 4*f* states overlap, influenced by the 3*d*–5*d* and 3*d*–4*f* hybridizations. From the magnetic measurements result that the investigated $Gd_{1-x}Ce_xCo_2$ compounds are ferrimagnetically ordered, with an antiparallel alignment between Gd and Co moments. The Curie temperature and the Co magnetic moments have been determined observing a descendent trend for both as the Ce concentration increases. These behaviours were attributed to the changes in the neighbourhood of the Co atoms through substitution of Gd for Ce which modify the contributions associated with R 5*d*–M 3*d* hybridization and finally the cobalt magnetic moment. The broad and almost symmetrical shape of the magnetic entropy changes, $\Delta S_M(T)$, peaks point out that the compounds exhibit a second-order magnetic phase transition. The relative cooling power (*RCP*) and normalized cooling power to the applied magnetic field (*RCP/ΔS)* have been calculated in order to evaluate the magnetic cooling efficiency

$GdCo_{2-x}A_x$ compounds (A = Ni, Mn, Cu and Al) possess cubic $MgCu_2$ - Laves type structure. The calculated lattice parameters are very close to those reported for $GdCo_2$. Band structure calculations for these compounds confirm very well the total magnetic moments per formula unit obtained experimentally. Furthermore, the atomic average magnetic moments for Gd, Co, Ni, Mn, Cu and Al were calculated. XPS measurements for $GdCo_{2-x}A_x$ compounds showed no significant shift in the binding energy of the investigated Co core levels with the change of the dopant element, as expected considering that the lattice parameter and hence the distance between the atoms have close values. For all investigated samples the Co 3*s* core level spectra give us direct evidence of the local magnetic moments on Co sites and an average magnetic moment atom can be estimated being, the values obtained being in very good agreement with the values obtained from band structure calculations and magnetic measurements. From the Mn 3*s* core level spectra an approximate value of the manganese magnetic moment was obtained. The magnetic measurements show that all of the samples are ferrimagnetically ordered. Moreover, the Arrott plots, the temperature dependence of Landau coefficients and the shapes of magnetic entropy changes confirm the presence of a second order magnetic phase transition. The calculated relative cooling power, RCP(S), normalized relative cooling power at the applied magnetic field, RCP(ΔS)/ΔB, and temperature-averaged entropy change, TEC parameters show that these compounds could be promising candidates for applications in magnetic refrigeration devices.

Bibliography

[1]. J.M.D. Coey, *Novel Permanent Magnetic Materials. Phys. Scr.*, T39, 21–28, 1991; J.M.D. Coey, *Perspective and Prospects for Rare Earth Permanent Magnets. Engineering*, 6, 119–131, 2020.

[2]. Y. Zhang, Review of the structural, magnetic and magnetocaloric properties in ternary rare earth RE_2T_2X type intermetallic compounds. *J. Alloys Compd.*, 787, 1173–1186, 2019.

[3]. Y. Wang, D. Guo, B. Wu, S. Geng, Y. Zhang, Magnetocaloric effect and refrigeration performance in $RE_{60}Co_{20}Ni_{20}$ (RE = Ho and Er) amorphous ribbons. *J. Magn. Magn. Mater.*, 498, 166179, 2020.

[4]. L. Li, M. Yan, Recent progresses in exploring the rare earth based intermetallic compounds for cryogenic magnetic refrigeration. *J. Alloys Compd.*, 823, 153810, 2020.

[5]. A. Brown, J.M. Westbrook, *Formation Technique*, 1967

[6]. H.M. Rietveld, A profile refinement method for nuclear and magnetic structures. *J.Appl. Cryst.*, 2, 65, 1969

[7]. M. Cardona L. Ley (editors), *Photoemission in Solids I*, Topics in Applied Physics vol. 26, Berlin: Springer, 1978

[8]. S. Hüfner, *Photoelectron Spectroscopy Principles and Applications*. Springer-Verlag, Berlin, Germany, 1995.

[9]. B. D. Cullity and C. D. Graham. *Introduction to Magnetic Materials*. John Wiley & Sons, Inc., Hoboken, New Jersey, 2009 .

[10]. J. Kohanoff, *Electronic Structure Calculations for Solids and Molecules: Theory and Computational Methods*. Cambridge University Press, 2006 .

[11]. J. Hubbard, Electron correlations in narrow energy bands - IV. The atomic representation. *Proc. R. Soc. Lond.*, 285, 542- 560, 1965.

[12]. V. I. Anisimov, J. Zaanen, and O. K. Andersen, Band theory and Mott insulators: Hubbard U instead of Stoner. *Phys. Rev. B*, 44, 943-954, 1991.

[13]. E. Burzo, Magnetic and crystallographic properties of rare-earth-- and yttrium--iron laves phases. *Z. Angew. Physik* 32, 127, 1971.

[14]. K. H. J. Buschow and R. P. van Stapele, Magnetic properties of the intermetallic compounds RFe_2. *J. de Physique Colloques*, 32, C 1-672, 1971 .

[15]. H. R. Kirchmayr and C. A. Poldy, Magnetism in rare earth-3d intermetallics. *J. Magn. Magn. Mater.*, 8, l, 1978.

[16]. F. Grandjean, G. D. Waddill, T. R. Cummins, D. P. Moore, G.J. Long and K. H.J. Buschow, A cerium M-edge X-ray absorption study of the CeM_2 compounds, where M is Mg, Al, Fe, Co, Ni, Ru and Rh. *Solid State Commun.* 108, 593, 1998 .

[17]. O. Eriksson, L. Nordstrom, M. S. S. Brooks and B. Johansson, 4f-Band Magnetism in $CeFe_2$. *Phys. Rev. Lett.* 60**,** 2523, 1988 .

[18]. S. J. Kennedy and B. R. Coles, The magnetic phases of pseudobinary $Ce(Fe_{1-x}M_x)_2$ intermetallic compounds; M=Al, Co, Ru. *J. Phys.: Condens. Matter* 2, 1213, 1990 .

[19]. L. Paolasini, P. Dervenagas, P. Vulliet, J-P Sanchez, G.H. Lander, A. Hiess, A. Panchula and P. Canfield, Magnetic response function of the itinerant ferromagnet $CeFe_2$. *Phys. Rev. B*, 58, 12117, 1998.

[20]. T. Fujiwara, H. Fujii, Y. Ishii, S. Koiwai, M. Kosaka, Y. Uwatoko, M. Nishi and K. Kakurai, Evidence of the anisotropically developed antiferromagnetic spin fluctuation in $CeFe_2$ under high pressures, *Physica B*, 312–313, 336, 2002.

[21]. L. Paolasini, B. Ouladdiaf, N. Bernhoeft, J.-P. Sanchez, P. Vulliet, G.H. Lander, and P. Canfield, Magnetic Ground State of Pure and Doped $CeFe_2$, *Phys. Rev. Lett.* 90, 057201, 2003 .

[22]. Tang C C, Chen D F, Li Y X, Wu G H, K. C. Jia and W. S. Zhan, Magnetic properties in Laves phase $Ce_xDy_{1-x}Fe_2$ intermetallics. *J. Appl. Phys.*, 82, 4424, 1997 .

[23]. C. C. Tang, W. S. Zhan, D. F. Chen, Y. X. Li, J. Du, B. G. Shen and G. H. Wu, Anomalous magnetic properties of cerium ions in the compounds $Ce_xR_{1-x}Fe_2$ (R = Tb, Dy). *J. Phys.: Condens. Matter*, 10, 2797, 1998 .

[24]. C. C. Tang, Y. X. Li, J. Du, G. H. Wu and W. S. Zhan Effects of rare-earth substitution in $CeFe_2$: mixed-valence and magnetic properties. *J. Phys.: Condens. Matter* 11, 2027, 1999 .

[25]. E. Burzo, H. R. Kirchmayr, A. Chelkovski, *Landolt Börnstein Handbuch*, vol. 192, Springer Verlag, 1990.

[26]. W. J. Feng, M. Gao, H. Zhang and Y. He, Structure, Magnetic Properties and Magnetocaloric Effect of Dy-Doped $CeFe_2$ Alloys. *Advanced Materials Research*, 700, 75, 2013 .

[27]. X. J. Wu, W. J. Feng, X. S. Sun, H. Chen and M. Gao, Reversible magnetocaloric effects and critical behaviors in $Ce_{1-x}Pr_xFe_2$ *Physica B*, 517 42, 2017 .

[28]. S. F. da Cunha, A. P. Guimaraes and F. P. Livi, Magnetic properties of the pseudo-binary intermetallic compounds (Ce_xY_{1-x}) Fe_2. *J. Phys. Chem. Solids* 41, 761, 1980 .

[29]. N. H. Duc and T. D. Hien, Magnetic properties of $(Ce,R)(Fe,Al)_2$ compounds. *J. Magn. Magn. Mater.*, 140-144, 1113, 1995.

[30]. J. Rodríguez-Carvajal, Recent advances in magnetic structure determination by neutron powder diffraction. *Phys. B Phys. Condens. Matter.*, 192, 55–69, 1993 .

[31]. G. Souca, R. Dudric, P. Vlaic, R. Tetean, Effects of Y doping on the magnetic properties and magnetocaloric effect of $CeFe_2$. *Materials Research Express*, vol. 6, 106122, 2019.

[32]. O. K. Andersen, Linear methods in band theory. *Phys. Rev. B* 12 3060, 1975.

[33]. O. K. Andersen and O. Jepsen, Explicit, First-Principles Tight-Binding Theory. *Phys. Rev. Lett.* 53, 2571, 1984.

[34]. S. H. Vosko, L. Wilk and M. Nusair. Accurate spin-dependent electron liquid correlation energies for local spin density calculations: a critical analysis. *Can. J. Phys.*, 58, 1200, 1980.

[35]. P. E. Blöchl, O. Jepsen and O. K. Andersen, Improved tetrahedron method for Brillouin-zone integrations. *Phys. Rev. B*, 49 16223, 1994 .

[36]. H. R. Kirchmayr, C. A. Poldy, R. Groessinger, R. Haferl, G. Hilscher, W. Steiner and G. Wiesinger *Magnetic properties of intermetallic compounds of rare earth metals (Handbook on the Physics and Chemistry of Rare Earths* **2** 55*)* (North-Holland Publishing Company)1979.

[37]. J. G. M. Armitage, T. Dumelow, P. C. Riedi and J. S. Abell The magnetic moment at the yttrium site in Y-Fe compounds: pressure dependence of the magnetisation and hyperfine field. *J. Phys.: Condens. Matter* 1, 3987, 1989.

[38]. K. W. Zhou, Y. H. Zhuang, J. Q. Li, J. Q. Deng and Q. M. Zhu, Magnetocaloric effects in $(Gd_{1-x}Tb_x)Co_2$. *Solid State Commun.*137, 275, 2006 .

[39]. P.D. Johnson, Y. Liu, Z. Xu, D.J. Huang, Spin Polarized Photoemission Studies of the 3s Core Levels in Fe and Co. *J. Electron. Spectrosc. Relat. Phenom.*, 75, 245, 1995 .

[40]. E. Burzo, Paramagnetic Behavior of Some Rare-Earth Cobalt Compounds. *Phys. Rev. B*, 6, 2882, 1972.

[41]. E. Burzo, D.P. Lazar, On the cobalt-induced moments in ternary gadolinium-yttrium compounds. *J. Sol. State Chem.*, 16, 257, 1976 .

[42]. E. Burzo, R. Tetean, Z. Sarkozi, L. Chioncel, M. Neumann, Magnetic properties and electronic structures of $RCo_{2-x}Si_x$ (R=Gd, Y) compounds. *J. Alloys Compds*., 323–324, 490, 2001 .

[43]. T. F. Smith, H. L. Luo, M. B. Maple, I. R. Harris, Superconductivity and magnetic susceptibility studies of the cubic Laves phase alloys $CeRu_{2-X}Co_x$. *J. Phys. F*, 1, 896, 1971 .

[44]. L. Pauling, The Nature of the Interatomic Forces in Metals. Phys. Rev., 54, 899, 1938.

[45]. R. Dudric, G. Souca, K. Kuepper, and R. Tetean, XPS on $Gd_{1-x}Ce_xCo_2$ Intermetallic Compounds, *Phys. Stat. Sol. B*, 256, 2, 1800320, 2018.

[46]. O. Gunnarsson and K. Schönhammer, *Handbook of Physics and Chemistry of Rare Earths*, Vol 10, Elsevier, Amsterdam, Holland 1987.

[47]. J. W. Allen, S. J. Oh, O. Gunnarsson, K. Schönhammer, M. B. Maple, M. S. Torikachvili, I. Lindau, Electronic structure of cerium and light rare-earth intermetallics. *Adv. Phys.*, 35, 275, 1986.

[48]. L. Braicovich, N. B. Brookes, C. Dallera, M. Salvietti, G. L. Olcese, High-energy Ce-3d photoemission: Bulk properties of CeM_2 (M=Fe, Co, Ni) and Ce_7Ni_3. *Phys. Rev. B*, 56, 15047, 1997.

[49]. J. C. Fuggle, F. U. Hillebrecht, Z. Zołnierek, R. Lässer, Ch. Freiburg, O. Gunnarsson, K. Schönhammer, Electronic structure of Ce and its intermetallic compounds. *Phys. Rev. B*, 27, 7330, 1983.

[50]. Y. Baer, Ch. Zürcher, Electronic Structure of CeN Studied by X-Ray-Photoemission Spectroscopy. *Phys Rev Lett*, 39, 956, 1977.

[51]. A. Popescu, O. Isnard, R. Dudric, M. Coldea, X-ray photoelectron spectroscopy and magnetic properties of $Ce_2Co_{15}Mn_3$ compound. *J Alloys Compds.*, 535, 10, 2012.

[52]. R. Dudric, A. Popescu, O. Isnard, M. Coldea, X-ray photoelectron spectroscopy and magnetic properties of $CeCo_7Mn_5$ and $CeCo_8Mn_4$ isostructural $ThMn_{12}$ type compounds. *Intermetallics*, 38, 150, 2013.

[53]. D. G. Van Campen, L. E. Klebanoff, Spin-resolved and high-energy-resolution XPS studies of the 3s and 2s levels of metallic cobalt. *Phys. Rev. B*, 49, 2040, 1994.

[54]. G. Chiaia, P. Vavassori, L. Dub, L. Braicovich, M. Qvarford, I. Lindau, Surface electronic structure of $CeCo_2$, $CeRh_2$ and $CeRh_3$ probed by valence band resonant photoemission spectroscopy. *Surface Science*, 331-333, 1229, 1995.

[55]. H. Ohta, M. Sumikawa, K. Kita, M. Motokawa, T. Seixas, M. Machado da Silva, Submillimeter wave ESR and magnetization measurements of $Ce_xGd_{1-x}Co_2$. *Physica B*, 216, 341, 1996.

[56]. K. Binder and A. P. Young, Spin glasses: Experimental facts, theoretical concepts, and open questions. *Rev. Mod. Phys*, 58, 801, 1986.

[57]. E. Burzo, Crystallographic, magnetic, and EPR studies of rare-earth and yttrium-cobalt laves phases. *Int.J.Magn.* 3, 161, 1972.

[58]. D. Givord, R. Lemaire, Magnetic Transition and Anomalous Thermal Expansion in R_2Fe_{17} Compounds. *IEEE Trans. Magn.* 10, 109–113, 1974 .

[59]. K. Fujiwara, K. Ichinose, A. Tsujimura, The Magnetic Properties of $GdCo_2$ Compound and Its Hydrides. *J. Phys. Soc. Japan.*, 56, 2149–2152, 1987.

[60]. T. Kaneko, K. Marumo, S. Miura, G. Kido, S. Abe, H. Yoshida, K. Kamigaki, Y. Nakagawa, High-field susceptibility of pseudobinary compounds $Gd(Co_{1-x}Ni_x)_2$. *Phys. B+C*, 149, 334–339, 1988 .

[61]. K. N. R.Taylor, Intermetallic rare-earth compounds. *Advances in Physics*, 20(87), 551–660, 1971 .

[62]. V. I. Gavrilenko, R. Q. Wu, Magnetostriction and magnetism of rare earth intermetallic compounds: First principle study. *J. Appl. Phys.* 89, 7320–7322, 2001 .

[63]. W. Zhong, W. Chen, W. Ding, N. Zhang, Y. Du, Q. Yan, Magnetocaloric properties of Na-substituted perovskite-type manganese oxides. *Solid State Commun.*, 106, 55–58, 1998 .